UNIVERSIDADE
BEIRA INTERIOR

SQUISH BAND INFLUENCE ON A PISTON PORTED 2-STROKE ENGINE PERFORMANCE

(Versão final após defesa)

Vítor Alexandre Pinheiro Silva

Dissertação para obtenção do Grau de Mestre em
Engenharia Aeronáutica
(Ciclo de estudos integrado)

Orientador: Prof. Doutor Francisco Miguel Ribeiro Proença Brójo

Maio de 2025

Declaração de Integridade

Eu, Vítor Alexandre Pinheiro Silva, que abaixo assino, estudante com o número de inscrição 39098 de/o Engenharia Aeronáutica da Faculdade de Engenharia, declaro ter desenvolvido o presente trabalho e elaborado o presente texto em total consonância com o **Código de Integridades da Universidade da Beira Interior**.

Mais concretamente afirmo não ter incorrido em qualquer das variedades de Fraude Académica, e que aqui declaro conhecer, que em particular atendi à exigida referenciação de frases, extratos, imagens e outras formas de trabalho intelectual, e assumindo assim na íntegra as responsabilidades da autoria.

Universidade da Beira Interior, Covilhã 6 / 5 /2025

Acknowledgements

First, I would like to thank both my parents, Vítor Silva and Sílvia Oliveira, for always believing in me and for the sacrifices made my entire life, allowing me to follow whatever path I intended with full support and encouragement. Also, to my sister Carolina Silva, for the motivation and inspiration to always continue forward and never give up.

I also want to thank my supervisor Professor Francisco Brójo for the guidance provided throughout this work and for the permanent availability and patience to help and encourage.

Finally, I want to thank the rest of my family for their support and my friends that accompanied me and turned this into the amazing journey that I will remember forever.

Resumo

Motores a dois tempos são utilizados mundialmente em aplicações onde um design leve, uma alta relação potência-peso e simplicidade são essenciais. O setor aeronáutico não é uma exceção, especialmente em veículos aéreos não tripulados (VANTs) e aeronaves ultraleves, onde uma alta relação potência-peso é crucial para o desempenho. Os avanços tecnológicos continuam a melhorar o seu desempenho, consolidando os motores a dois tempos como uma parte confiável e indispensável tanto na aviação como no setor de transportes como um todo.

Este estudo realizado tem como objetivo analisar a influência da "squish band" na eficiência de combustão e no desempenho de motores a dois tempos. Para isso, foi projetado do zero um pequeno motor a dois tempos com 50cc e admissão controlada pelo pistão, que serviu como base para as análises. A "squish band" do motor projetado foi alterada em três características diferentes: a folga deixada até ao pistão em ponto morto superior (PMS), o ângulo da "squish band" e a percentagem da área do pistão com influência da "squish band". Com estas modificações, foram criadas e analisadas seis variações diferentes do motor base.

As simulações numéricas foram realizadas no ANSYS Fluent. Neste software CFD, o movimento dos componentes ao longo do ciclo, bem como a circulação das substâncias e a combustão, foram modelados e as diferentes simulações foram realizadas. Os resultados revelaram que o motor projetado demonstrou o desempenho esperado e as diferentes variações da "squish band" proporcionaram resultados interessantes.

Palavras-chave

CFD, Fluent, Dois-tempos, Combustão interna, Admissão controlada pelo pistão, Ignição por faísca, CAD, Squish Band, Desempenho

Abstract

Two-stroke engines are widely used worldwide in applications where lightweight design, high power-to-weight ratio, and simplicity are essential. Common modern uses include motorcycles, marine engines, and small machinery. In the aeronautical sector, they are especially valuable in unmanned aerial vehicles (UAVs) for both civilian and military purposes, where their high power-to-weight ratio is critical for performance. They are also used in ultralight aircraft, aeromodelling, and experimental aviation due to their compact design and cost-effectiveness. Advances in technology continue to improve their performance, solidifying two-stroke engines as a reliable and indispensable part of both aviation and the entire transport sector.

This study intends to analyse the influence of the squish band on the combustion efficiency and performance of two-stroke engines. For that, a small 50cc two-stroke piston ported SI engine was designed from scratch to serve as the base for the analysis. The squish band of the designed engine was then altered in three different characteristics: the gap to the piston crown at top dead center (TDC), the angle of the squish band and the percentage of the piston's bore area where a squish band was present. With these modifications, a total of six different variations of the base engine were created and analysed.

The numerical simulations were performed in ANSYS Fluent. In this CFD software, the engine's motion through its cycle and the species movement and combustion were modelled and the different calculations were computed. The results revealed that the designed engine performed as expected and the different squish band variations provided interesting results.

Keywords

CFD, Fluent, Two-stroke, Internal Combustion (IC), Piston Ported, Spark Ignition, CAD, Squish Band, Performance

Contents

List of Figures

List of Tables

List of Acronyms

BDC	Bottom dead center
CAD	Computer aided design
CFD	Computational fluid dynamics
CI	Compression ignition
CV	Cylinder volume
DNS	Direct numerical simulation
IC	Internal combustion
LES	Large eddy simulation
MPA	Mean port area
PCR	Primary compression ratio
PISO	Pressure-Implicit with Splitting of Operators
RANS	Reynolds averaged Navier–Stokes
RPM	Revolutions per minute
SI	Spark ignition
TDC	Top dead center
UAV	Unmanned aerial vehicles
UBI	Universidade da Beira Interior
URF	Under-relaxation factors

Nomenclature

α	Crank angle	[deg]
B	Bore	[mm]
CR	Compression ratio	[-]
F	Force	[N]
l	Connecting rod length	[mm]
m	Mass	[Kg]
$\dot{m}$	Mass flow rate	[g/h]
N	Rotational velocity	[RPM]
P	Pressure	[Pa]
p	Power	[KW]
$\dot{q}$	Rate of volumetric heat addition per unit mass	[W/(Kg·m^3)]
ρ	Density	[Kg/m^3]
r	Crank radius	[mm]
R_{bs}	Bore-to-stroke ratio	[-]
R_{rs}	Rod-to-stroke ratio	[-]
S	Stroke	[mm]
sfc	Specific fuel consumption	[g/KW· h]
t	Time	[s]
θ	Port opening duration	[deg]
T	Torque	[N·m]
$\mathcal{V}$	Volume	[cc]
V	Velocity	[m/s]
V_c	Clearance volume	[cc]
V_{cc}	Crankcase clearance volume	[cc]
V_d	Displacement volume	[cc]
x_i	Substance mole fraction	[-]
n_i	Substance quantity	[mol]

Chapter 1

Motivation and Objectives

1.1 Motivation

The two-stroke engine has been a reliable and useful option ever since its invention in the 19^{th} century. Even in recent times with the advancements in four-stroke and electrical engines, the two-stroke engine retained its importance whenever a lightweight design, a high power-to-weight ratio or simplicity are crucial factors.

Two-stroke engines are extensively used in a wide range of industries varying from motorcycles and marine engines to small utility and hand machinery. In the aeronautical sector, they are especially valuable in unmanned aerial vehicles (UAVs) for both civilian and military purposes. Additionally in ultralight aircraft, aeromodelling and experimental aviation, their compact design, lightweight and cost-effectiveness make two stroke engines a worthy and common choice. Advances in technology, such as direct fuel injection and improved lubrication systems, continue to improve their performance, solidifying two-stroke engines as a reliable and indispensable part of both aviation and the transport sector.

Within a two-stroke engine's cycle, it is safe to say that the combustion process carries a crucial role in the overall performance of the engine. An efficient combustion leads to more power, better fuel economy, reduced emissions and improved reliability. As a result, optimizing the combustion process is a important step in the evolution of two-stroke engines. An important and impactful aspect of the combustion process in the squish band. The squish band is the outer area of the combustion chamber and, unlike the actual "dome", is shaped so as to be a short distance from the piston at top dead center (TDC).[14] A well designed squish band will improve the combustion process and so it is important to understand the effects it causes and how to properly implement them.

1.2 Objectives

With that in mind, the objective of this work is to understand the influence of the squish band in the combustion efficiency and performance of a two-stroke engine. In order to execute the intended analysis, first, a base engine design in which to perform the simulations was needed. So, a small 50cc piston ported SI two-stroke engine will be developed from scratch. To the base engine design, different variations of the squish band's dimensions will be implemented creating different configurations of the engine. Those configurations

will then be subjected to a numerical simulation in a CFD software. The results will, hopefully, reveal how the squish band influences a two-stroke engine's combustion process.

1.3 Outline

In the present chapter an explanation of the motivations behind this work and its objectives are presented. In the following chapter, chapter 2, a bibliographic review of the theory and concepts related to the topic in study is prepared. In chapter 3, the dimensioning process of the engine is explained, and the final engine geometry is presented. In chapter 4, the developed model for the numerical simulation is presented along with the geometry and mesh models for the six different tests to be performed. In chapter 5, the results from the simulations of the six tests are presented and discussed. Finally, in chapter 6, a final overview of the work done is presented and the final considerations are made.

Chapter 2

Bibliographic Review

2.1 History on two stroke engines

It is generally accepted that the two-stroke cycle engine was invented by Sir Dugald Clerk in England at the end of the 19^{th} Century.[3] However, the lightweight and simple design we recognize today was developed by Joseph Day. Working with his assistant Frederick Cock, Day modified his original ”valveless air compressor” to create a new design where the piston controlled the inlet port. This innovation, called the ”valveless two-stroke engine,” utilized the crankcase compression for the induction process and the piston to regulate the opening and closure of the exhaust, transfer, and intake ports.

Initially, two-stroke engines were primarily used in motorcycles, but over time, their compact size and lightweight design made them the preferred choice for applications where these factors are critical. Today, two-stroke engines are found in a wide range of devices, including ATVs, snowmobiles, jet skis, power tools, generators, remote-controlled models, and more.[18]

Recent advancements, such as direct fuel injection and supercharging, have significantly improved the efficiency of two-stroke engines. These developments are particularly impactful in the UAV industry, where hybrid applications are now being explored.

2.2 Two-stroke engine operation and components

A two-stroke engine generates power through two piston movements (strokes) per power cycle: one upward and one downward. This differs from a four-stroke engine, which requires four separate movements (intake, compression, power, and exhaust).[17] In a two-stroke engine, these processes are combined into two steps:

1. **Compression Stroke (Upstroke):** The piston moves upward, compressing the fresh air-fuel mixture drawn into the cylinder during the previous downstroke. Near the top dead center (TDC), the spark plug ignites the compressed mixture, starting combustion.

2. **Power Stroke (Downstroke):** The ignited air-fuel mixture rapidly increases pressure and temperature, driving the piston downward and generating power. As the piston moves down, it uncovers the exhaust port, allowing burnt gases to escape. Almost simultaneously, the transfer port opens, letting fresh air-fuel mixture from the crankcase enter the cylinder. This process of clearing the exhaust gases and filling the cylinder with fresh mixture for the next cycle is called scavenging.

The cycle repeats every two strokes of the piston, figure (2.1)

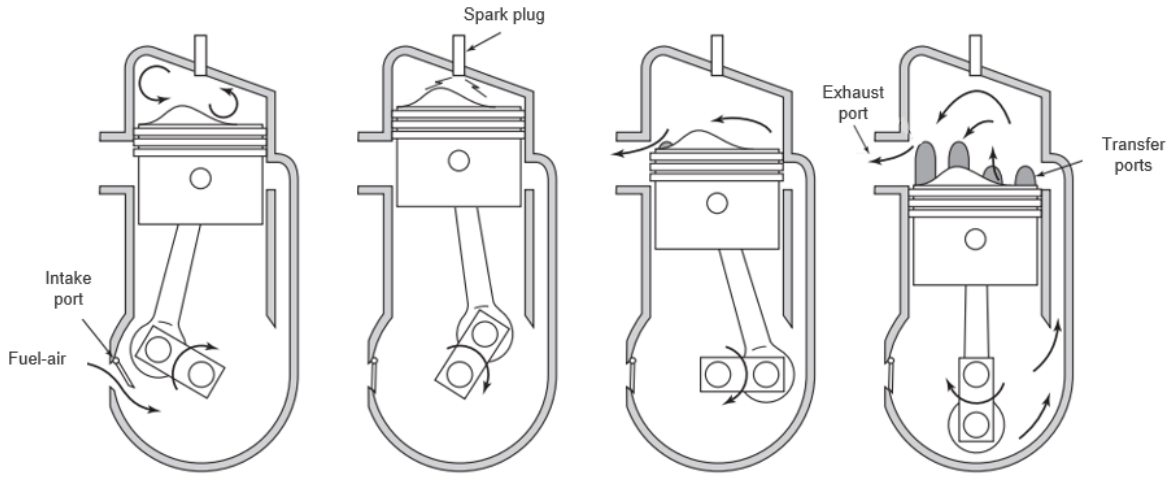

Figure 2.1: Typical two stroke engine geometry and cycle. Adapted from [6].

A common two-stroke engine usually has the following major components.

- **Piston:** Moves up and down inside a cylinder, creating a sealed chamber where fuel and air are mixed and combusted. Also transfers the force from the expanding gases to the crankshaft. This downward motion is what ultimately drives the crankshaft. Essentially, the piston converts the energy from the combustion process into mechanical energy.
- **Cylinder / Liner:** Is a cylindrical chamber that houses the piston and provides the space for it to move up and down.
- **Block:** Overall, the engine block forms the core structure of the engine, providing the frame where the rest of the components are attached. Is typically made of cast iron or aluminium alloy in order to have a good strength, durability and ability to dissipate heat efficiently.[11]
- **Crankshaft:** It's the component responsible for converting the linear motion from the piston into rotational motion.
- **Connecting Rod:** Connects the piston to the crankshaft.

- **Combustion Chamber:** Is located between the piston crown and the cylinder head and its where the combustion process occurs.
- **Ports:** Openings in the cylinder wall that allow the flow of air-fuel mixture and exhaust gases in and out of the cylinder. There are three types of port:
  - Intake port: Transports the fresh air/fuel mixture into the crankcase.
  - Transfer ports: Are responsible for transferring the fresh air/fuel mixture from the crankcase to the cylinder.
  - Exhaust port: Transports burned gases out of the cylinder after combustion.

2.2.1 Timing Diagram

To obtain a working and efficient two-stroke engine, is crucial to optimise its timing diagram. A timing diagram, is a portrait of the processes that occur in a two-stroke engine cycle by the piston covering and uncovering ports in the cylinder wall. Figure (2.2) shows a typical timing diagram on two-stroke engines and bellow is an interpretation of this diagram.

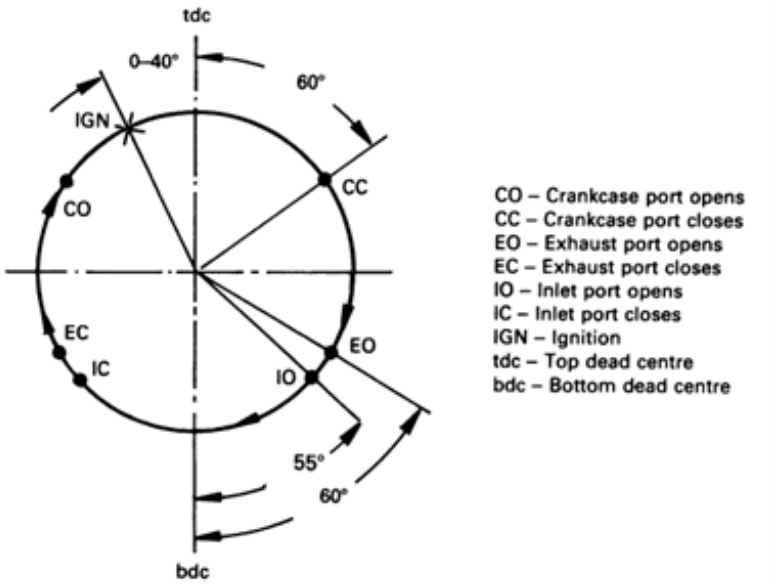

Figure 2.2: Typical timing diagram of a piston ported two-stroke engine. Adapted from [19].

1. At about 60° before bottom dead center, the piston uncovers the exhaust port (EO). [19] This point marks the end of the power stroke.

2. Some 5-10° later the inlet port is opened (IO) and the charge compressed by the underside of the piston in the crankcase is able to flow into the cylinder. [19]

3. The scavenge process ends once the inlet port is closed (about 55° after bottom dead center) (IC). [19]

4. At about 60° after bottom dead center the exhaust port is closed (EC), and the charge is compressed by the upward motion of the piston. [19]

5. At about 60° before top dead center the pressure in the crankcase is significantly below the ambient pressure, and the intake port opens (CO) to allow the incoming charge to flow into the crankcase. [19]

6. Ignition (IGN) occurs typically within the range of 10°-40° before top dead center. [19] This point marks the beginning of the power stroke.

7. The intake port is closed (CC) about 60° after top dead center. [19].

2.2.2 Piston and Piston Rings

The piston is a critical component in any combustion engine serving multiple purposes in its operation. The main role of the piston is compressing the air-fuel mixture in the cylinder, preparing it for an efficient combustion. At the same time, the piston both seals the cylinder and transmits the combustion-generated gas pressure to the crank pin via the connecting rod [5] enabling the conversion to mechanical power. In specific two-stroke engines the piston carries an additional role of acting like a valve, controlling the opening and closing of the ports.
There are several designs of pistons each with its merits. The **flat-top piston** is the simpler design. As the name suggests the top of the piston is flat meaning a simple manufacturing process whilst maintaining an adequate performance overall. The **dome-top piston** is the same as a flat top piston but with a dome shaped top. This allows it to reduce the engine's compression ratio allowing for a better performance. On the other hand, this design has a more complex and expensive manufacturing process. The **deflector piston** is a design that enables a better scavenging process because of a raised deflector on the top of the piston that directs the fresh charge towards the top of the combustion chamber and away from the exhaust port. This design carries an even more complex manufacturing process and cost but usually improves both the engine's performance and fuel efficiency. These are the most common piston designs utilized in two-stroke engines. The selection of the right type of piston for each engine needs to be a compromise between performance, durability, fuel efficiency and scavenging system as well as manufacturing costs.

Piston rings are essential components located on the sides of the piston, playing a crucial role in engine performance. Their primary functions include:

- Sealing the combustion chamber by creating a tight seal between the piston and cylinder wall, improving efficiency.
- Regulating oil flow to the combustion chamber, reducing smoke emissions and excessive oil consumption.
- Transferring heat from the piston to the cylinder wall, preventing overheating.
- Minimizing component wear by reducing direct metal-to-metal contact.

There are three main types of piston rings: **compression rings** that ensure a good seal of the combustion chamber, **oil control rings**, which regulate oil passage between the piston and cylinder wall and **scraper rings** that remove excess oil from the cylinder wall.[12]
Designing an effective piston ring is challenging, as it must be flexible to expand and contract, withstand high stress and heat, and, especially in two-stroke engines, move smoothly over ports without snagging or breaking.

2.2.3 Connecting Rod and piston pin

The connecting rod is a mechanical component that converts linear motion into rotary motion. It connects the piston to the crankshaft and transmits the force resultant from the combustion process to the crankshaft creating the rotation power output of the engine. A usual connecting rod is composed of three zones: the **big end**, the side that attaches to the crankshaft and rotates on a bearing, the **small end**, is on the other side and attaches to the piston via a piston pin and the **shank**, the long middle section, typically shaped for optimal weight and strength balance.

The design process of a connecting rod is based in stress resistance and a low weight compromise because, the perfect connecting rod is one that complies with its objective of force transmission and stability without adding too much weight to the engine. It is usually made of steel or alloy forging in most engines but may be aluminum in some small engines [15].

The piston pin is typically made of steel or alloy and is usually hollow to reduce its weight. [5] It needs an appropriate resistance to stress in order to safely connect the connecting rod and the piston throughout the engine's cycle.

2.2.4 Cylinder and Combustion Chamber

The cylinder is a fundamental component of an engine. It houses the piston assembly allowing for its movement up and down during each engine cycle and, on two stroke engines, also houses the transfer and exhaust ports. The walls of the cylinder have highly polished hard surfaces. Cylinders may be machined directly in the engine block, or a hard metal (drawn steel) sleeve may be pressed into the softer metal block.[15] A well designed cylinder must be able to sustain stress from the piston's movement and the combustion process and also dissipate heat effectively in order to maintain a airtight seal with the piston rings ensuring a proper compression and consequently an effective combustion.

The combustion chamber is the space at the top of the cylinder, between the cylinder head and the piston face where combustion occurs. The size of the combustion chamber continuously changes from a minimum volume when the piston is at TDC to a maximum when the piston is at BDC. [15]

The cylinder head seals off the cylinder and is made of cast iron or aluminum. It must be strong and rigid to distribute the gas forces acting on the head as uniformly as possible through the engine block. The cylinder head contains the spark plug (in a SI engine) or the fuel injector (in a CI engine). [5]

2.2.5 Squish Band

The squish band is located around the edge of the combustion chamber and is designed to come very close to the piston crown at TDC, figure (2.3).

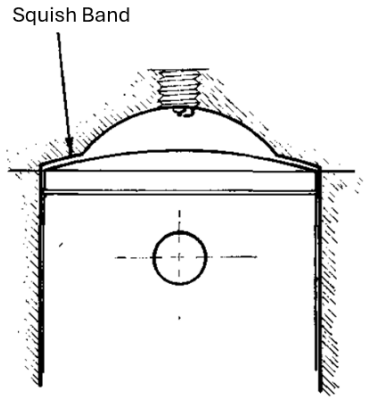

Figure 2.3: Squish band on a two-stroke engine. Adapted from [2].

Its name comes from one of its primary functions: to "squish" the air-fuel mixture toward the center of the combustion chamber. This allows the fast moving gases to meet the spark plug and quickly carry the combustion flame to the extremity of the combustion chamber, thus preventing detonation. [2]

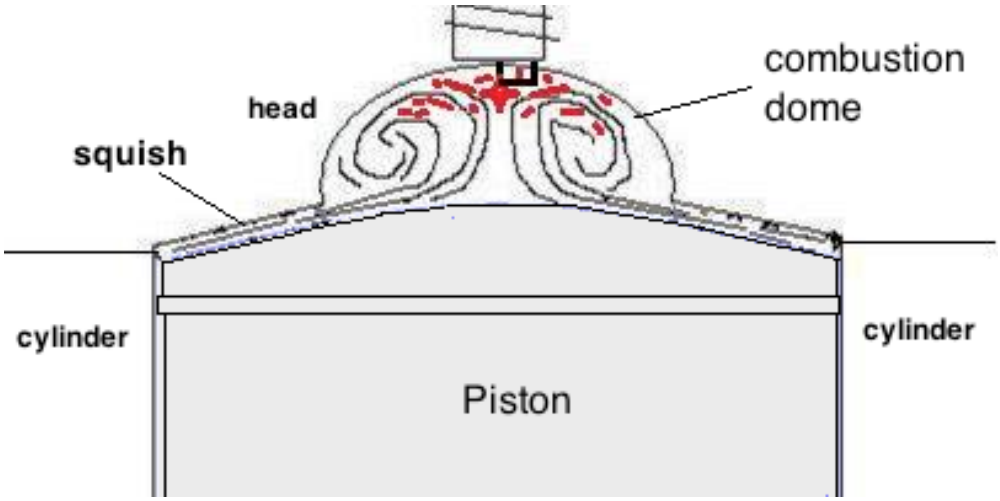

Figure 2.4: Squish band turbulent effect. Adapted from [7].

Further studies have shown that the turbulence generated by the squish band not only promotes better homogenization of the air-fuel mixture but also aids in mixing any remaining exhaust gases with the fresh charge. This results in faster, more complete, and more efficient combustion.

Additionally, the turbulence enhances heat transfer within the chamber. Without proper heat transfer, jets of flame would tend to shoot out toward the edges of the combustion chamber, prematurely heating the surrounding gases to start off the cycle leading to detonation.[2]

2.2.6 Port Shapes

The design and shape of the ports in two-stroke engines is crucial to its performance, efficiency, and power output. Unlike four-stroke engines, that use valves to control the intake and exhaust of gases, two-stroke engines rely on ports opening and closing with the piston's movement, making their shapes significantly affect how the air-fuel mixture and exhaust gases flow through the engine.

There are many different port shapes that can be used in a two-stroke engine. Rectangular based, cylindrical based or trapezoidal based ports can all be viable options depending on the case, figure (2.5). Overall, within each individual engine's restrictions, we want the shape that allows the best flow coefficient for any timing-area value. In most cases that result is obtained with the widest port [9].

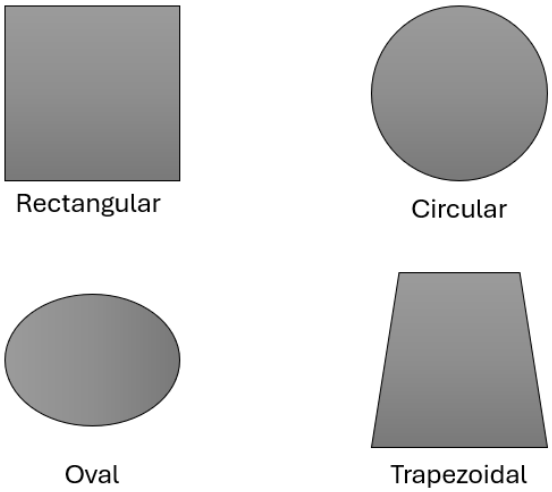

Figure 2.5: Typical port shapes.

Intake Port

Typically located on the side or bottom of the crankcase. Its shape is often a rectangular or trapezoidal slot to ensure the optimal flow of the fuel-air mixture. A wider port will, in most cases, provide the best flow coefficient but widening the port also has its consequences. A very wide port can cause the bottom edge of the piston skirt to snag at the bottom of the port window [9]. Rounding the corners of the port can help with this issue, but an overly wide port will eventually cause a more rapid wear of the piston skirt.

Exhaust Port

The exhaust port is the highest on the cylinder wall. A well-designed port will provide efficient exhaust scavenging, enhancing the engine's power output and preventing exhaust gases from mixing with the incoming air-fuel mixture. The same principle applied for the intake port is true for the exhaust port, increasing the width will result in an increase of power but, for the same reasons, a drastic decrease in ring life. Enlarging the port so that its width is 70-percent of cylinder bore diameter, ring failure would almost certainly occur during the first revolution of the crankshaft [9]. For these reasons, a compromise must be achieved between a good flow coefficient and ring life expectancy when designing the exhaust port.

Transfer ports

When it comes to designing and optimizing the transfer ports, a few things should be considered. The shape is less important than in the previous ports because transfer ports are not usually wide enough to cause any considerable ring damage, it is important however to carefully design the shape and angle of the duct. Transfer ports are critical in allow-

ing the fresh mixture to come in the cylinder and push out the exhaust gases. It is then important to select the appropriate scavenging method for the engine in question before designing the transfer port because factors like angle and even number of ports are dependent on what method is chosen. When dealing with an engine with multiple transfer ports it is crucial to guarantee that the distance between the exhaust port's side-wall and the forward edge of the transfer port is not decreased below .350-inch [9] which is when short-circuiting the fresh charge becomes a problem [9]. Short-circuiting the charge refers to the circumstance in which some portion of the fresh air-fuel mixture escapes directly out of the exhaust port without contributing to the combustion.

2.2.7 Crankshaft

The crankshaft has three main functions: converting the linear (up and down) motion of the piston into rotational motion, transmitting the power output of an engine to the load and balancing the forces acting on the engine.[16] It is connected to the engine block and to the connecting rod with bearings.[15] The crankshaft is typically made of forged steel, cast iron, or alloy materials to handle high stresses and temperatures and it is designed to resist bending, twisting, and fatigue over prolonged use.

2.2.8 Engine Geometry and Parameters

In figure (2.6) it is presented the geometric parameters of a usual engine assembly.

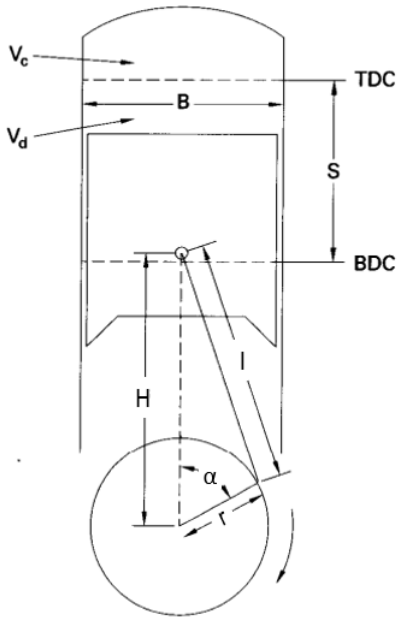

Figure 2.6: Typical engine geometry and parameters. Adapted from [5] [15]

Where B is the piston's bore (usually refers to the diameter of the piston), S is the stroke (distance the piston travels inside the cylinder, from TDC to BDC), l is the connecting rod length, r is the crank radius, α is the crank angle, V_d is the displacement volume and V_c is the clearence volume. From these parameters, some relations can be made.

Geometrically, the crank radius must be one-half of the piston stroke, equation (2.1),

$$S = 2r \quad (2.1)$$

A determining factor of an engine's design is it's **bore to stroke ratio (R_{bs})**, equation (2.2):

$$R_{bs} = \frac{B}{S} \quad (2.2)$$

An engine with a R_{bs} lower than 1, where the stroke is larger than the piston's bore, is said to be 'undersquare'. On the other hand, an R_{bs} higher than 1 classifies the engine as 'oversquare' and if the R_{bs} is approximately equal to 1 the engine is 'square'. Generally, oversquare engines are more inclined towards high performance uses, square engines towards general-purpose small engines and undersquare for heavy-duty low-speed, high-torque engines.

The **Rod to stroke ratio**, equation (2.3), plays a significant role in the performance characteristics of the engine, such as its power delivery, efficiency, and longevity.

$$R_{rs} = \frac{l}{S} \quad (2.3)$$

Typical values for R_{rs} vary depending on the intended objective of the two-stroke engine:

- $1.8 < R_{rs} < 2.2$ for high-performance racing engines. [5]
- $1.4 < R_{rs} < 1.8$ for utility and small engines. [5]
- $1.2 < R_{rs} < 1.4$ for larger, low-speed, torque-oriented engines. [5]

The **compression ratio**, equation (2.4), is the ratio of the cylinder's maximum volume (with the piston at BDC) to the cylinder's minimum volume (with the piston at TDC).

$$CR = \frac{Cylinder\ Volume\ at\ BDC}{Cylinder\ Volume\ at\ TDC} \quad (2.4)$$

It can also be described as seen in equation (2.5).

$$CR = \frac{V_d + V_c}{V_c} \quad (2.5)$$

A high compression ratio has always been equated with high horsepower [2], so high performance two-stroke engines typically have higher compression ratios (6:1 to 8:1) for increased power, while general-purpose and utility engines often have lower compression ratios (5:1 to 7:1) for durability and lower-risk operation. Finally, engines designed for torque and fuel efficiency at lower RPM's usually have the lowest compression ratio (4:1 to 6:1).

2.2.9 Scavenging

Scavenging is the process of removing exhaust gases from the combustion chamber and simultaneously filling it with a fresh air-fuel mixture. In a four-stroke engine, the intake and exhaust strokes are separated but for a two-stroke engine both need to be merged. This overlap means that fresh air-fuel mixture is introduced while exhaust gases are still being expelled causing an effective scavenging to become crucial to ensure that all burnt gases are expelled from the cylinder and fresh mixture is properly introduced to prepare for the next combustion cycle. These reasons put scavenging in an essential role, maintaining engine efficiency and power output.

Scavenging begins when, as the piston moves downward after combustion, the exhaust port opens, allowing burnt gases to exit the cylinder.[8] Slightly after, the piston's movement uncovers the transfer ports and fresh air-fuel mixture is pushed from the crankcase into the cylinder, typically aided by the downward motion of the piston increasing the pressure in the crankcase. The fresh mixture entering the cylinder pushes the remaining exhaust gases out through the exhaust port. The piston then moves back up (compression stroke), covering both the transfer ports and the exhaust port, trapping the fresh charge in the cylinder for the next combustion cycle.

Throughout the years different methods for cylinder scavenging were created, figure (2.7). **Cross scavenging** is an older design, where the transfer port and exhaust port are located directly opposite in the cylinder. This makes the fresh charge flow across the cylinder from one side to the other forcing the exhaust gases out. This design lacks efficiency because exhaust and intake gases cross paths, which can lead to poor scavenging efficiency and some fresh mixture being lost through the exhaust port.

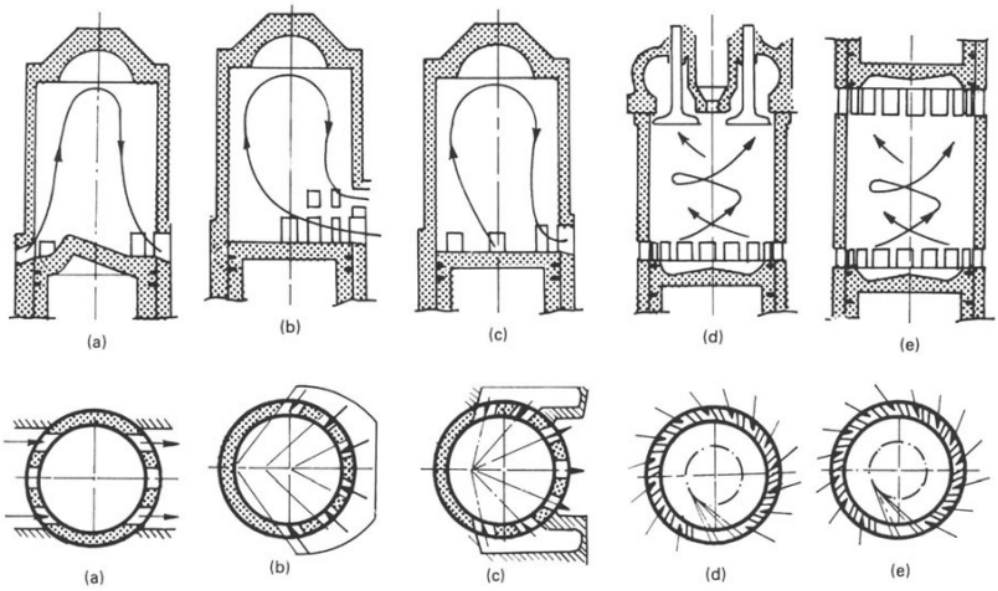

Figure 2.7: The different scavenging arrangements and the associated port geometry for two-stroke engines: (a) cross-scavenging; (b) loop scavenging; (c) Schnurle loop scavenging; (d) uniflow scavenging with poppet exhaust valves; (e) uniflow scavenging with opposed pistons. [19]

Loop Scavenging is a more modern design where the exhaust port sits higher up in the cylinder compared to the transfer port. This way, the fresh mixture loops inside the cylinder and pushes the exhaust gases out through the exhaust port above. Compared to the cross-scavenging method this one is more efficient as it minimizes the loss of fresh charge through the exhaust port.

The **Schnuerle loop scavenging** is a modified version of the loop scavenging system that was designed to improve the efficiency of valveless two-stroke engines. For this method the transfer port is split in two angled ports, one in each side of the exhaust port. This increases scavenging efficiency and has been almost universally adopted by makers of high output two-stroke engines [9].

Uniflow scavenging is the most efficient type and commonly used in large, primarily diesel, engines. Fresh air-fuel mixture enters from the bottom while exhaust gases exit from a valve at the top of the cylinder, resulting in a one-way flow.

A good scavenging process needs to eliminate all the exhaust gases and replace them with fresh air-fuel mixture while preventing the new charge to be lost through the exhaust port. All this needs to be done in one piston stroke which makes scavenging a complex process. A effective scavenging process is critical because it improves engine performance, power output, and fuel efficiency, while poor scavenging can lead to incomplete combustion and higher emissions.

2.2.10 Fuel and Ignition Systems

On two-stroke engines there are two different types of ignition system that depend on the type of engine, it's purpose and especially the type of fuel it uses. The first method is ignition by an external source, such as a spark plug, called **Spark Ignition (SI)**. The second is ignition by compression of the charge or autoignition, called **Compression Ignition (CI)**.

Compression Ignition (CI)
In a two-stroke CI engine, air is drawn into the cylinder and compressed to a high pressure and high temperature. Fuel is then injected into the hot, high-pressure air, where it autoignites and proceeds with the combustion process. This type of engines require a specific type of fuel, usually diesel fuel because of its low volatility and low ignition temperature.

Spark Ignition (SI)
In two-stroke SI engine, a mixture of air and fuel is introduced to the cylinder where it is then compressed. These engines rely on an electric spark to initiate combustion of the fuel/air charge which has been inducted into the cylinder. For the engine to operate efficiently, the spark must be delivered at precisely the right moment in relation to the position of the piston in the cylinder and the rotational speed of the crankshaft. [2] In SI engines usually gasoline is the utilised fuel because of its high volatility and ability to mix with air in a homogeneous mixture.

2.2.11 Cooling System

On an average two-stroke engine, some type of cooling system is required to remove approximately 30% of the fuel energy rejected as waste heat, liquid and air cooling are the two main types of cooling systems. [6]

Air Cooling System
This cooling method relies on air flowing over the engine's surface to dissipate heat. The cylinder head and block are equipped with fins that increase surface area, enhancing heat dissipation. Cooling occurs either naturally (passive cooling) or with the help of a fan (forced-air cooling).

Air cooling is the simplest method, as it requires no additional components. It is especially common in smaller, portable two-stroke engines.

Liquid Cooling System
In this method, liquid coolant (usually a mix of water and antifreeze) is circulated through the engine cylinder and head to absorb heat and then cooled in a radiator. The coolant circulates through cooling jackets and a water pump is often used to assist its movement.

This system is used in high performance engines as it provides a more effective and consistent cooling, the downside is that it adds an additional complexity to the engine, requiring a radiator and sometimes a water pump making it a heavier and more expensive option when compared to the air-cooling system.

2.2.12 Performance Parameters

There are countless ways of analysing a two-stroke engine performance but two parameters stand out from the rest and those are:

Power and torque: Power is the measure of the engine's ability to produce mechanical power, usually measured in horsepower (HP) or kilowatts (kW). Torque is the rotational force generated by the engine and is typically measured in Newton-meters (Nm). The relation between the two is represented in equation (2.6) where p is the power, T is the torque and N is the engine's speed in revolutions per minute (RPM).

$$p = \frac{2\pi \times N \times T}{60} \quad (2.6)$$

Specific fuel consumption (sfc): Is a measure of the efficiency of an engine in using fuel to produce power. A smaller sfc value means a more efficient engine, meaning that less fuel is being consumed to produce the same power output.

$$sfc = \frac{\dot{m}_f}{p} \quad (2.7)$$

Where, $\dot{m}_f$ is the fuel mass flow rate in (g/h) and p the power output in (kW). The specific fuel consumption is expressed in $(g/kW \cdot h)$.

2.2.13 Emissions

In an ideal combustion of a hydrocarbon only CO_2 and H_2O are produced. However, in the real-world, this combustion reaction is not perfect and, along with them, other products may be created such as carbon monoxide (CO), nitrogen oxides (NO_x), additional unburned hydrocarbons (HC) and particulate matter (PM). These undesired products are usually prevenient from an incomplete combustion, high combustion temperatures or unintended lubrication oil combustion. These emissions are extremely harmful for the environment and, among others, contribute to global warming, air pollution, water pollution and even ecosystem damage. Because of this, now more than ever, restrictions on engines emissions and extensive legislation are in course in order to mitigate the pollution crises the world faces at the moment.

2.3 Computational Fluid Dynamics (CFD)

Computational Fluid Dynamics (CFD) is a branch of fluid mechanics that uses numerical methods and algorithms to solve and analyse problems involving fluid flow, heat transfer, and other related phenomena. Fluid dynamics is basically the investigation of the interactive motion of a large number of individual particles, like molecules or atoms. Because of this, it must be assumed that the density of the fluid is high enough, so that it can be approximated as a continuum [4]. CFD allows engineers and scientists to simulate the behaviour of fluids in various conditions and environments without the need for physical testing, which can be expensive, time-consuming, and sometimes impractical.

Focusing on the mathematics behind CFD and the equations it implements is not the purpose of this thesis, nonetheless, a short overview of the set of equation on the heart of fluid dynamics and the numerical algorithms behind CFD softwares, such as the one utilized in chapter (4), is important knowledge and, for that reason, with the help of the guidelines done in [4] and [10], a brief study will be done in this next section.

2.3.1 Governing Transport Equations

At the core of CFD are the **Navier-Stokes equations**, which describe how fluids behave. They are the mathematical statements of three fundamental physical principals upon which all of fluid dynamics is based [10]:

- Conservation of mass.
- Conservation of momentum.
- Conservation of energy.

In obtaining the basic equations of fluid motion, the following philosophy is always followed [10]:

- Choose the appropriate fundamental physical principles from the law of physics such as:
  - Mass is conserved
  - F=ma (Newton's second law)
  - Energy is conserved
- Apply these physical principles to a suitable model of the flow.
- From this application, extract the mathematical equations which embody such physical principles.

The governing equations can be obtained in various different forms, considering a finite control volume will lead to final integral equations while considering an infinitesimally small volume will lead to final partial differential equations. At the same time, considering a fixed volume with the fluid moving through it, will provide the final equations in conservation form and considering a volume moving with the fluid will provide equations in nonconservation form. In the end, whether we deal with each form of the equations is irrelevant. Indeed, through simple manipulation, one form can be obtained from the other. [10] Knowing this, obtaining the governing equations will be done utilizing the infinitesimally small volume moving with the flow, figure (2.8d).

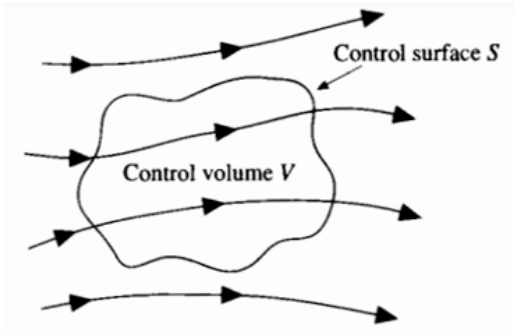

(a) Finite control volume fixed in space.

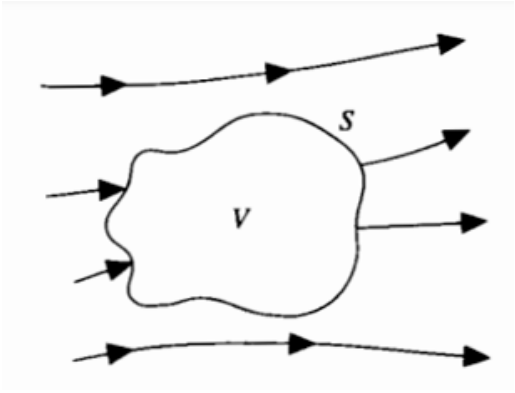

(b) Finite control volume moving with the fluid.

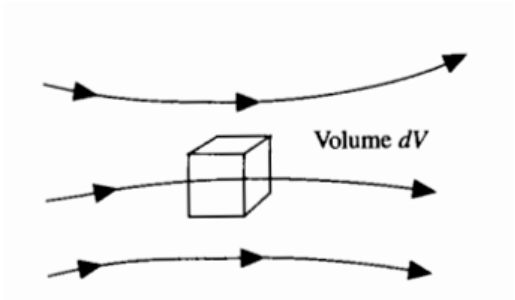

(c) Infinitesimal fluid element fixed in space.

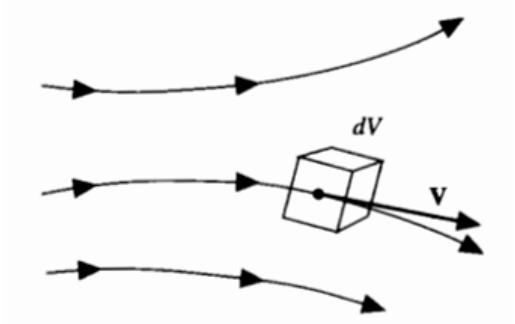

(d) Infinitesimal fluid element moving along the flow.

Figure 2.8: Models of a flow. Adapted from [10]

Conservation of mass

Applying the philosophy mentioned above, in this case the physical principal is the law of mass conservation that expresses the fact that mass cannot be created in such a fluid system, nor can disappear from it.[4]

The element in question has a fixed mass, but its shape and volume will change as it moves downstream. So, with a fixed mass δm and variable volume $\delta \mathcal{V}$ follows that:

$$\delta m = \rho \, \delta \mathcal{V} \quad \textbf{(2.8)}$$

Since mass is conserved, as the element moves along with the flow it's time rate of change of mass is zero.

$$\frac{D(\delta m)}{Dt} = 0 \quad \textbf{(2.9)}$$

So, combining equations (2.8 and 2.9), equation (2.10) is obtained.

$$\frac{D(\rho \, \delta \mathcal{V})}{Dt} = \delta \mathcal{V} \frac{D\rho}{Dt} + \rho \frac{D(\delta \mathcal{V})}{Dt} = 0 \quad \textbf{(2.10)}$$

Simplifying:

$$\frac{D\rho}{Dt} + \rho \left[\frac{1}{\delta \mathcal{V}} \frac{D(\delta \mathcal{V})}{Dt} \right] = 0 \quad \textbf{(2.11)}$$

Recognizing the term in brackets as the physical meaning of $\nabla \cdot \mathbf{V}$, equation (2.12) is obtained which is the partial differential equation form of the continuity equation.

$$\boxed{\frac{D\rho}{Dt} + \rho \nabla \cdot \mathbf{V} = 0} \quad \textbf{(2.12)}$$

Conservation of momentum

Following the same philosophy as before, the physical principle applied now is Newton's second law, which goes as follows in equation (2.13) considering only the x component.

$$F_x = m a_x \quad \textbf{(2.13)}$$

F_x represents the forces experienced on the element, and in this case they come from two distinct sources:

Body forces: which act directly on the volumetric mass of the fluid element, for example gravitational, electric and magnetic forces. These are represented in equation (2.14),

$$\text{Body force (x)} = \rho f_x (dx\, dy\, dz) \quad (2.14)$$

Surface forces: which act directly on the surface of the fluid element and are due to two sources, pressure distribution on the surface and shear and normal stress distributions. This way, the surface forces are represented in equation (2.15).

$$\begin{aligned}\text{Net x surface force } = &\left[p - \left(p + \frac{\partial p}{\partial x}dx\right)\right] dy\, dz + \left[\left(\tau_{xx} + \frac{\partial \tau_{xx}}{\partial x}dx\right) - \tau_{xx}\right] dy\, dz \\ &+ \left[\left(\tau_{yx} + \frac{\partial \tau_{yx}}{\partial y}dy\right) - \tau_{yx}\right] dx\, dz + \left[\left(\tau_{zx} + \frac{\partial \tau_{zx}}{\partial z}dz\right) - \tau_{zx}\right] dx\, dy\end{aligned} \quad (2.15)$$

The sum of equations (2.14 and 2.15) is the total force in the x direction, F_x:

$$F_x = \left[-\frac{\partial p}{\partial x} + \frac{\partial \tau_{xx}}{\partial x} + \frac{\partial \tau_{yx}}{\partial y} + \frac{\partial \tau_{zx}}{\partial z}\right] dx\, dy\, dz + \rho f_x\, dx\, dy\, dz \quad (2.16)$$

Now, considering that the mass of the fluid element is fixed and the acceleration of the fluid element is the time rate of change of its velocity, comes equation (2.17):

$$a_x = \frac{Du}{Dt} \quad (2.17)$$

From combining equations (2.16 and 2.17) into equation (2.13) equation (2.18) is obtained which is the x component of the momentum equation. The y and z components are obtained similarly and are represented in equations (2.19 and 2.20) respectively.

$$\boxed{\rho \frac{Du}{Dt} = -\frac{\partial p}{\partial x} + \frac{\partial \tau_{xx}}{\partial x} + \frac{\partial \tau_{yx}}{\partial y} + \frac{\partial \tau_{zx}}{\partial z} + \rho f_x} \quad (2.18)$$

$$\boxed{\rho \frac{Dv}{Dt} = -\frac{\partial p}{\partial y} + \frac{\partial \tau_{xy}}{\partial x} + \frac{\partial \tau_{yy}}{\partial y} + \frac{\partial \tau_{zy}}{\partial z} + \rho f_y} \quad (2.19)$$

$$\boxed{\rho \frac{Dw}{Dt} = -\frac{\partial p}{\partial z} + \frac{\partial \tau_{xz}}{\partial x} + \frac{\partial \tau_{yz}}{\partial y} + \frac{\partial \tau_{zz}}{\partial z} + \rho f_z} \quad (2.20)$$

Conservation of energy

Similarly to the above equations, the physical principle now applied is the first law of thermodynamics that, when aplyed to the model element, states that the rate of change of energy inside the fluid element must equal the net flux of heat into the element plus the rate of work done on the element due to body and surface forces.[10]

The rate of work done by the **body force**, for a fluid element moving at a velocity V can be represented by expression (2.21).

$$\rho \mathbf{f} \cdot \mathbf{V}(dx\, dy\, dz) \quad (2.21)$$

In terms of the rate of work done by the **surface forces**, in this case, pressure and shear and normal stresses must be accounted for. Expression (2.22) considers these forces in the x direction. For the y and z directions, similar ones are obtained.

$$\left[-\frac{\partial(up)}{\partial x} + \frac{\partial\left(u\tau_{xx}\right)}{\partial x} + \frac{\partial\left(u\tau_{yx}\right)}{\partial y} + \frac{\partial\left(u\tau_{zx}\right)}{\partial z}\right] dx\, dy\, dz \quad (2.22)$$

Combining the expressions of all directions mentioned above, with the body force effect from (2.21), equation (2.23) is obtained which is the rate of work done on the moving fluid element due to body and surface forces.

$$\begin{aligned} \text{rate of work} \\ \text{body/surface forces} \end{aligned} = -\Bigg[\left(\frac{\partial(up)}{\partial x} + \frac{\partial(vp)}{\partial y} + \frac{\partial(wp)}{\partial z}\right) + \frac{\partial\left(u\tau_{xx}\right)}{\partial x} + \frac{\partial\left(u\tau_{yx}\right)}{\partial y} + \frac{\partial\left(u\tau_{zx}\right)}{\partial z} + \frac{\partial\left(v\tau_{xy}\right)}{\partial x} + \frac{\partial\left(v\tau_{yy}\right)}{\partial y} + \frac{\partial\left(u\tau_{zy}\right)}{\partial z} + \frac{\partial\left(w\tau_{xz}\right)}{\partial x} + \frac{\partial\left(w\tau_{yz}\right)}{\partial y} + \frac{\partial\left(w\tau_{zz}\right)}{\partial z}\Bigg] dx\, dy\, dz + \rho \mathbf{f} \cdot \mathbf{V} dx\, dy\, dz \quad (2.23)$$

For the net flux of heat into the element, volumetric heating, such as absorption or emission of radiation, and heat transfer across the surface, from temperature gradients, must be considered.

In terms of volumetric heating, being $\dot{q}$ the rate of volumetric heat addition per unit mass, follows that:

$$\text{Volumetric heating of element} = \rho \dot{q}\, dx\, dy\, dz \quad (2.24)$$

For the heat transfers across the surface, equation (2.25) represents the net heat transferred into the fluid element by thermal conduction.

$$\begin{matrix}\text{Heating of fluid element}\\ \text{by thermal conduction}\end{matrix} = -\left(\frac{\partial \dot{q}_x}{\partial x} + \frac{\partial \dot{q}_y}{\partial y} + \frac{\partial \dot{q}_z}{\partial z}\right) dx\, dy\, dz \quad (2.25)$$

Combining equations (2.24 and 2.25) the result is the net flux of heat into the element, represented in equation (2.26).

$$\begin{matrix}\text{Net flux of heat}\\ \text{into the element}\end{matrix} = \left[\rho\dot{q} + \frac{\partial}{\partial x}\left(k\frac{\partial T}{\partial x}\right) + \frac{\partial}{\partial y}\left(k\frac{\partial T}{\partial y}\right) + \frac{\partial}{\partial z}\left(k\frac{\partial T}{\partial z}\right)\right] dx\, dy\, dz \quad (2.26)$$

Finally, the time rate of change of energy of the fluid element has two contributions, the internal energy, due to random molecular motion, and the kinetic energy, due to translational motion of the fluid element. This way, the term is the sum of the internal and kinetic energies, as represented in equation (2.27).

$$\begin{matrix}\text{Rate of change of energy}\\ \text{inside fluid element}\end{matrix} = \rho\frac{D}{Dt}\left(e + \frac{V^2}{2}\right) dx\, dy\, dz \quad (2.27)$$

As mentioned above, the rate of change of energy inside the fluid element must equal the net flux of heat into the element plus the rate of work done on the element due to body and surface forces. This way, combining the necessary expressions obtained in equations (2.23, 2.26 and 2.27) translates into equation (2.28) which is the partial differential equation form of the energy equation.

$$\begin{aligned}\rho\frac{D}{Dt}\left(e + \frac{V^2}{2}\right) = {} & \rho\dot{q} + \frac{\partial}{\partial x}\left(k\frac{\partial T}{\partial x}\right) + \frac{\partial}{\partial y}\left(k\frac{\partial T}{\partial y}\right) + \frac{\partial}{\partial z}\left(k\frac{\partial T}{\partial z}\right) - \frac{\partial(up)}{\partial x} - \frac{\partial(vp)}{\partial y} \\ & - \frac{\partial(wp)}{\partial z} + \frac{\partial\left(u\tau_{xx}\right)}{\partial x} + \frac{\partial\left(u\tau_{yx}\right)}{\partial y} + \frac{\partial\left(u\tau_{zx}\right)}{\partial z} + \frac{\partial\left(v\tau_{xy}\right)}{\partial x} + \frac{\partial\left(v\tau_{yy}\right)}{\partial y} \\ & + \frac{\partial\left(v\tau_{zy}\right)}{\partial z} + \frac{\partial\left(w\tau_{xz}\right)}{\partial x} + \frac{\partial\left(w\tau_{yz}\right)}{\partial y} + \frac{\partial\left(w\tau_{zz}\right)}{\partial z} + \rho\mathbf{f}\cdot\mathbf{V}\end{aligned} \quad (2.28)$$

2.3.2 Turbulent Flow Simulation

A century of experience has shown the 'turbulence problem' to be notoriously difficult, and there are no prospects of a simple analytic theory. Instead, the hope is to use the ever-increasing power of digital computers to achieve the objective of calculating the relevant properties of turbulent flows. [13] What makes a turbulent flow so hard to model is that it has a three-dimensional velocity field, it is time-dependent and random. There are distinct ways of tackling this turbulent flow problem.

- **Turbulent-flow simulation**, in which the equations are solved for a time-dependent velocity field that represents the velocity field. These approaches are:
  - **Direct numerical simulation (DNS)** where the Navier–Stokes equations are solved to determine U(x, t) for one realization of the flow. DNS is computationally expensive and restricted to flows with low-to-moderate Reynolds number.[13]
  - **Large eddy simulation (LES)** where equations are solved for a 'filtered' velocity field U(x, t), which is representative of the larger-scale turbulent motions. The equations solved include a model for the influence of the smaller-scale motions which are not directly represented.[13]
- **Turbulence model**, in which the equations are solved for mean quantities. These approaches are called **Reynolds averaged Navier–Stokes (RANS)**, since they involve the solution of the Reynolds equations to determine the mean velocity field (U). The Reynolds stresses, which appear as unknowns in the Reynolds equations, are determined by a turbulence model, either via the turbulent viscosity hypothesis or more directly from modelled Reynolds-stress transport equations.[13]
  - The best example of this approach is the $k - \varepsilon$ model, which is the most widely used complete turbulence model. It is generally regarded as being easy to use and computationally inexpensive making it the best option for accuracy at a relatively low computational demand.

Chapter 3

Engine Dimensioning

In order to analyse the influence of the squish band in an engines' performance, the first step was to design and dimensionalize a two-troke engine that would serve as the base in which the different analysis would be conducted. A two-stroke piston ported engine, in which the intake, exhaust and transfer ports were controlled by the pistons' movement, was the chosen layout and the objective was a small sized engine with a displacement of 50cc.

3.1 Piston and Cylinder

From literature the majority of 50 cc two-stroke engines use pistons with a bore in between 39mm and 43mm, so with this information a model with a 42.6mm bore was adopted. Determining the stroke can be achieved from equation (3.1).

$$S = \frac{V_d}{\pi(\frac{B}{2})^2} \quad (3.1)$$

Where S is the stroke, V_d is the total displacement of the engine and B is the pistons bore. Knowing the needed values, the stroke was calculated to be approximately 35.08mm.

Concerning the cylinder's design, it was necessary to obtain its length, and for that there isn't much information available in literature. Since the cylinder's objective is to seal the piston allowing for its movement and, at the same time, house the engine's ports, its length needs to be bigger than the stroke by a margin that allows a safe placement of the intake port. With this information and the value of the stroke, 35.08mm, a cylinder with a heigh of 59mm was created.

3.2 Crankshaft and Connecting Rod

With the value of the stroke calculated, the dimension of the crankshaft's radius must be half of it, as seen in section (2.2.8), in this case 17.54mm. This radius is measured from the center of the crankshaft to the crankpin, where it connects to the connecting rod.

As mentioned in section (2.2.8), for small utility two stroke engines, values for the rod to stroke ratio fall between 1.4 to 1.8. With this information, for this case a ratio of 1.5 was utilized arriving at a 52.62mm rod length.

3.3 Crankcase

The primary focus when designing the crankcase was its primary compression ratio (PCR), which can be calculated from equation (3.2). For small two stroke engines, PCR values usually fall between 1.2 and 1.5 [9]. So, for this case, a value 1.3 was utilized.

$$PCR = \frac{V_{cc} + V_s}{V_c} \quad (3.2)$$

Where, V_{cc} is the crankcase clearance volume (volume of the crankcase when the piston is at TDC) and V_s is the swept volume of the crankcase (volume displaced by the piston as it moves from TDC to BDC).

Knowing that, for this engine, V_s was approximately 50 cm^3, from equation (3.2) followed that the crankcase volume when the piston was at TDC needed to be around 166.67 cm^3. A simple cylindrical crankcase was than designed matching the previously obtained volume.

3.4 Ports

The dimensioning process of the ports shape and placement in the cylinder was based on literature, especially on Gordon Jennings - Two-stroke tuner's handbook [9], which has very detailed guidelines towards two-stroke engines port design. One of the guidelines provided by the author was an interval of admissible values for a well-designed intake, exhaust and transfer port.

- For piston controlled intake ports, 0.00014 to 0.00016 $s \cdot cm^2/cm^3$
- For transfer ports, 0.00008 to 0.00010 $s \cdot cm^2/cm^3$
- For exhaust ports, 0.00014 to 0.00015 $s \cdot cm^2/cm^3$

These are a reference to the values obtained from expression (3.3).

$$\frac{MPA}{CV} \times t \quad (3.3)$$

Where MPA is the mean port area, CV is the cylinder's volume and t is the total time the port stays open. Using expression (3.3) and the reference values provided it is now possible to properly design each of the necessary ports and the process is identical for each of the three different calculations.

As far as the mean port area is concerned, the first step was deciding on the shape of the ports. As seen in section (2.2.6), for piston ported engines, the best choice was an elongated hole, in order to help prevent an excessive wear on the piston rings. For these

reasons, the shape presented in figure (3.1) was the choice made for all the engines' ports. This meant that the mean port area was the area of the shape for each of the ports in study.

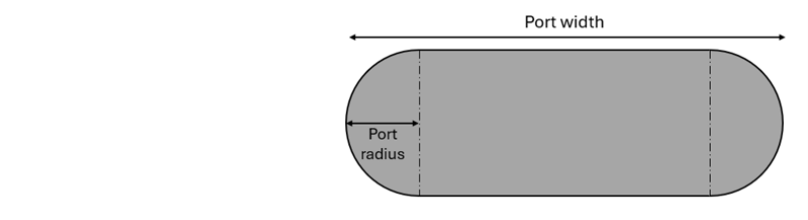

Figure 3.1: Layout of the shape of the ports

The total time the port stays open can be calculated from expression (3.4).

$$t = \frac{\theta}{N \times 6} \quad (3.4)$$

Where θ is the port opening duration in degrees and N is the rotational speed in (RPM) in which the engine is intended to develop maximum power. For this case $7000\ rpm$ was the assumed value as per the values from literature for similar engines.

With t properly defined and knowing the cylinder volume from section (3.1), the value from equation (3.3) was dependent only on the ports dimensions and it's opening duration θ. So, utilizing the software Microsoft Excel, more precisely the solver function, for each individual case it was possible to vary the variables until the result fitted the reference values provided earlier.

Intake port

For the intake port, it is recommended to use a port width of about 65% of the piston's bore. Based on this, the width for this case was defined as $2.769\ cm$. Then, as described above, utilizing the solver function from Microsoft Excel, the port's radius and opening duration θ was varied until the final value fell under the provided references. The final results produced a port radius of approximately $0.407\ cm$ and an opening duration θ of $160°$ for a final value from equation (3.3) of approximately $0.000144\ s \cdot cm^2/cm^3$.

Exhaust port

For the exhaust port, normal values for the width fall between $62\% - 70\%$ of the piston's bore. For this case, a width of $2.6412\ cm$ was used, a smaller value to help improve the life of the piston rings. Using the same process as for the intake, port radius and opening duration were varied until the values fell between the references provided, arriving at a final result of $0.449\ cm$ for the port's radius and $164°$ for the opening duration for a final value from (3.3) of approximately $0.00015\ s \cdot cm^2/cm^3$.

Transfer port

The transfer ports case was slightly different because there was a choice to be made of how many ports to have. In order to achieve a more evenly distributed and filled cylinder, thus improving combustion efficiency, power output and mixture flow, a pair of ports instead of just one was decided on. This difference means only that the mean port area is a combination of two ports instead of just the one. From this step, the same methodology as for the other ports was used and resulted in a $1.5\ cm$ width and a radius of $0.2825\ cm$ for each of the two ports and a total opening duration of $124°$. These dimensions produced a final result from equation (3.3) of $0.0000821\ s \cdot cm^2/cm^3$.

Table (3.1) summarises the final dimensions and duration of the engine's ports.

Table 3.1: Final dimensions of the engine's ports

	Width [cm]	**Radius [cm]**	**Opening duration [degrees]**
Intake	2.769	0.407	160
Exhaust	2.6412	0.449	164
Transfer	1.5	0.2825	124

Finally, the height where each of the ports sat on the cylinder needed to be calculated.

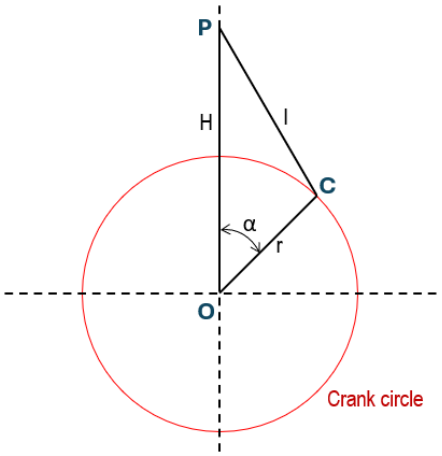

Figure 3.2: Port height in cylinder problem definition. Adapted from [20].

This problem is ilustrated in figure (3.2) and from there equation (3.5) was obtained.

$$H = r \times \cos(\alpha) + \sqrt{l^2 - r^2 \times \sin(\alpha)^2} \quad (3.5)$$

From which, knowing the opening duration of the ports θ and subsequently the opening duration from TDC α, the crank radius r and the connecting rod length l,H,the height for each of the angles to the piston pin, could be calculated.

Finally, the value of $H_{exhaust}$ and $H_{transfer}$ plus the distance from the piston pin to the top of the piston, in this case $20\ mm$, gives the final height for the exhaust and transfer

ports. For the intake port, the final height is H_{intake} minus the distance from the piston pin to the bottom of the piston, in this case $8\ mm$. From [9] explains that the exhaust port is considered open when 75% of its area is uncovered, the intake when 50% is uncovered and the transfer port when 70% is uncovered. Based on these indications, the height calculated above coincides with the line where each port is considered open.

3.5 Final components and assembly design

After all the components were properly idealized and dimensioned, with the help of CAD software CATIA V5, the final configuration of the base engine's design was computed. Below, in figures (3.3, 3.4, 3.5, 3.6, 3.7 and 3.8) and in appendix (A.1) the final results of the drawn components and the final product assembly are shown.

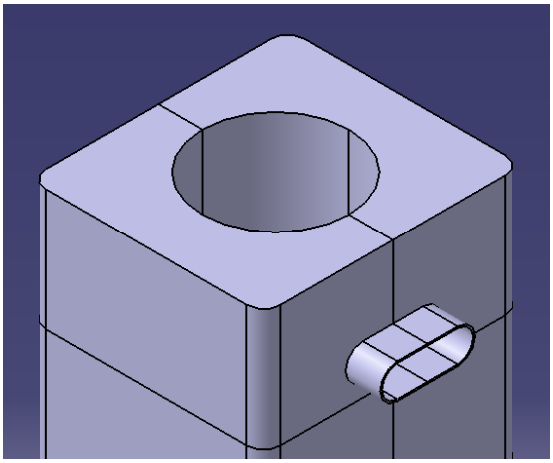

Figure 3.3: Isometric view of the cylinder.

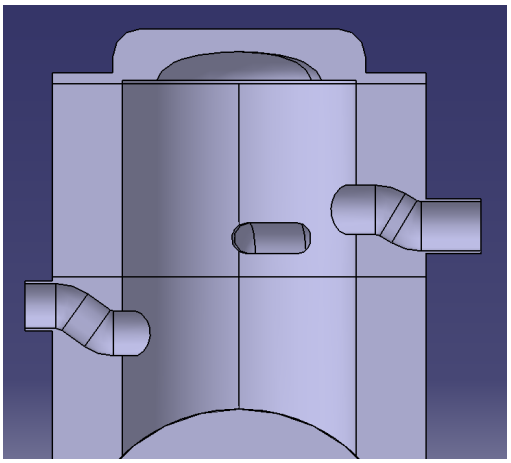

Figure 3.4: Interior of the cylinder and ports locations.

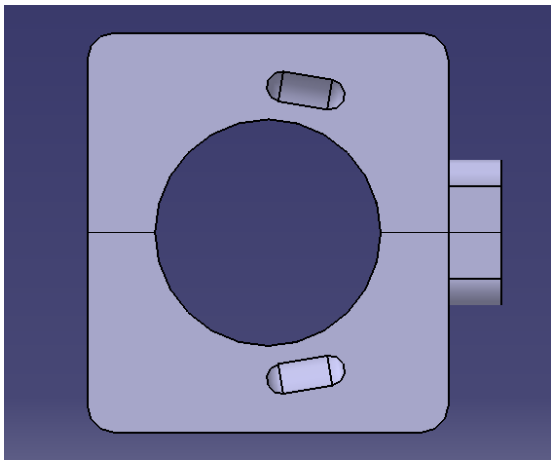

Figure 3.5: Bottom view of the cylinder and transfer ports.

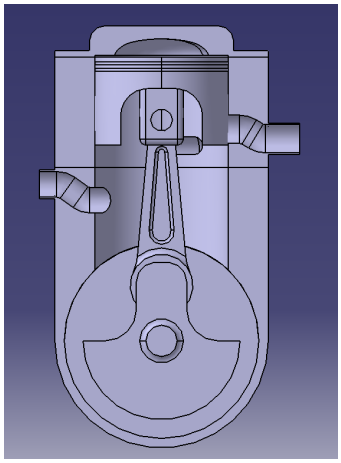

Figure 3.6: Full interior design with components.

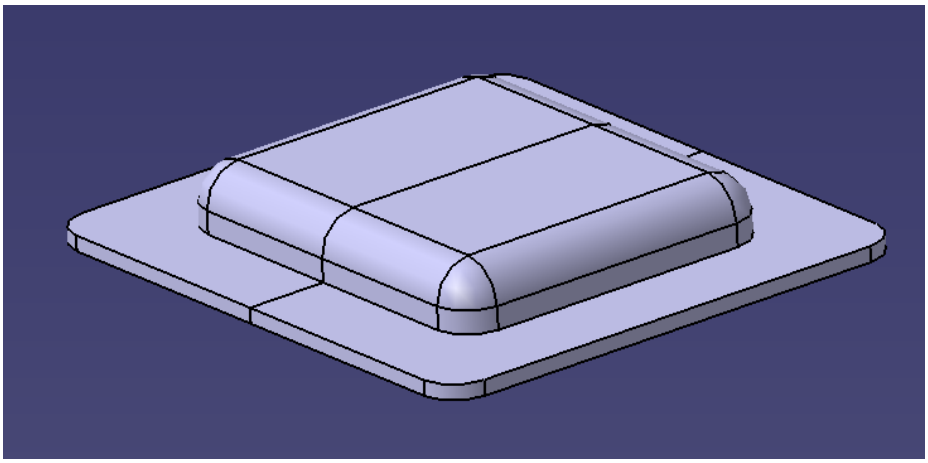

Figure 3.7: Isometric view of the engine head design.

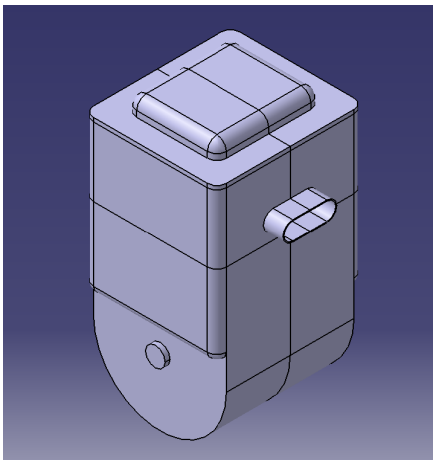

Figure 3.8: Isometric view of the full engine design.

Chapter 4

Numerical Simulation

4.1 Analysis Definition

With the base engine designed, the next step was determining what parameters to vary in order to understand the influence of the squish band in the engine's performance. The decision was to vary three different constraints of the squish band. First, the gap left between the squish band and the top of the piston at TDC, as seen in figure (4.1a). Second, the angle of the squish band, meaning the inclination from the outer portion of the cylinder towards the combustion chamber, figure (4.1b). Finally, the last variation is the percentage of the piston's bore area where a squish band is present, figure (4.1c).

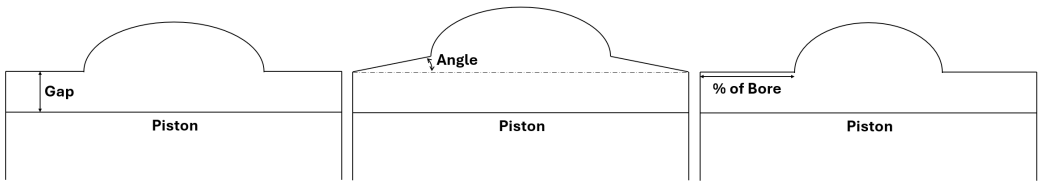

(a) (b) (c)

Figure 4.1: Layout of the analysis variables.

4.2 CFD Software

With the objective of the analysis well defined, the software ANSYS, more precisely FLUENT was the chosen platform for the analysis. Because of its accuracy, robustness and ease of use, FLUENT is a preferred choice for engineers and researchers and for these reasons the software was the ideal choice. Modelling an entire engine's cycle and combustion is a demanding task both in terms of time and computational power so, in order to improve the analysis efficiency and after initial tests, a choice was made of removing the crankcase and restricting the geometry to start at the meeting point of the transfer ports and the crankcase this way, the overall complexity of the model is reduced without considerable influence in the final results.

4.3 Test Layout, Geometry and Mesh

A total of four different tests were to be made. A base test, named test-0, serving as the starting point and comparison ground for the remaining evaluations. A test-1, where the gap (4.1a) is reduced and the rest remains constant, a test-2 varying only the angle of the

squish band, (4.1b), and a test-3 altering the percentage of area where the squish band is present,(4.1c). After the conclusion of these initial four tests, an additional two were performed varying multiple constraints simultaneously, In test-4, both the gap and angle of the squish band were modified and finally, in test-5, all the constrains were altered.

4.3.1 Mesh

For the meshing process, there are two distinct zones to take into account. The ports, transfer and exhaust, will remain identical for all the tests and so their mesh will be the same throughout the different analysis. For these ports a structured prism mesh was chosen and it can be seen in figure (4.2) while the full mesh parameters are in table (B.1 in App.B).

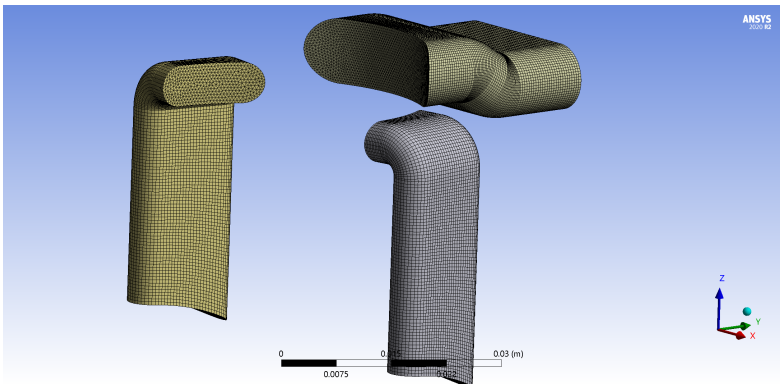

Figure 4.2: Mesh view of the ports.

The engine head on the other end, will be different in every test because of the changes to the squish band. To maintain an identical simulation environment, the same mesh configuration will be applied to all the different engine head variations. While defining it, it is important to consider that the cylinder's mesh will vary with the movement of the piston throughout its cycle. Because of this, the mesh needed to be built in structured layers to allow the nodes to split and collapse easily, which can be seen in figure (4.3). The complete configuration and parameters of this mesh can be consulted in table (B.2 in App.B).

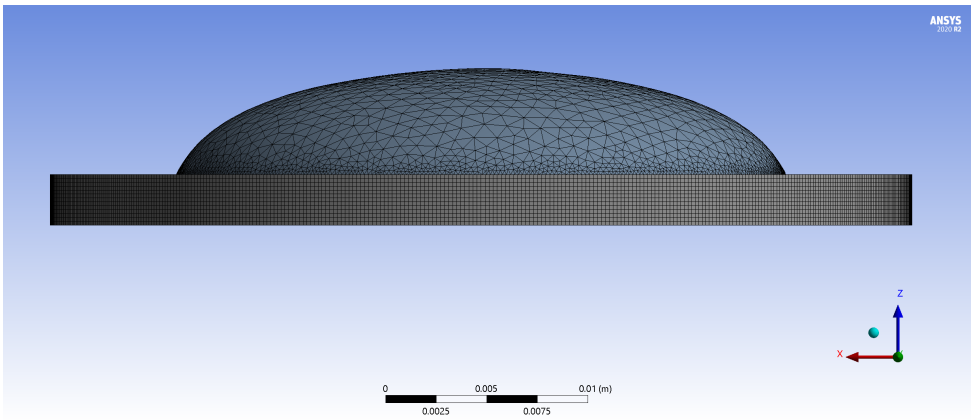

Figure 4.3: Structured layered mesh for the cylinder.

In figure (4.4) a full model mesh is represented. In this case, the model is for the test-0 simulation and the resulting mesh consists of 802751 nodes and 1252776 elements. These numbers will remain similar for the mesh of every model variation, although they represent only the initial configuration of the mesh because, with the dynamic mesh implemented, the number will increase until the piston reaches BDC and then return to the initial position.

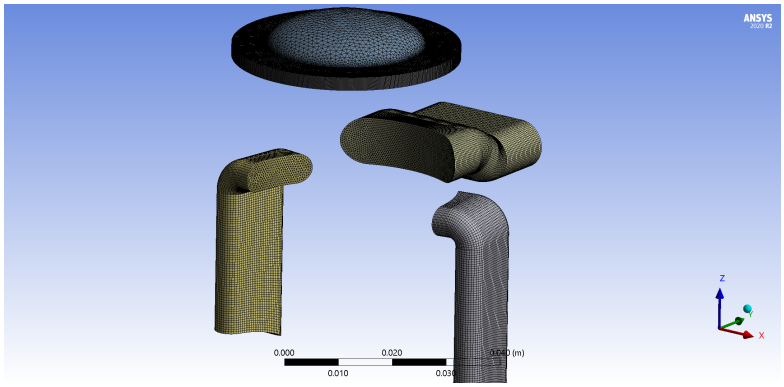

Figure 4.4: Mesh view of the full model for test-0.

4.3.2 Test-0

As mentioned, this test serves as the comparison ground for the other tests acting as a benchmark for their results. The geometry is as designed in chapter (3) and the squish-band's parameters can be seen in table (4.1). With a bore of 21.3 mm the piston's bore area is $1425.31\ mm^2$ so the initial squish band was designed to cover about 50% of this area, which is an average value for two stroke engines, as mentioned in [9].

Table 4.1: Squish band parameters for test-0.

Gap [mm]	Angle [deg]	% of Bore Area
2.5	0	50

The mesh layout of this test's engine head can be seen in figure (4.6) and the full geometry model is presented in figure (4.5).

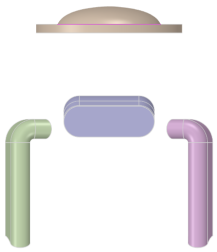

Figure 4.5: Geometry model for test-0.

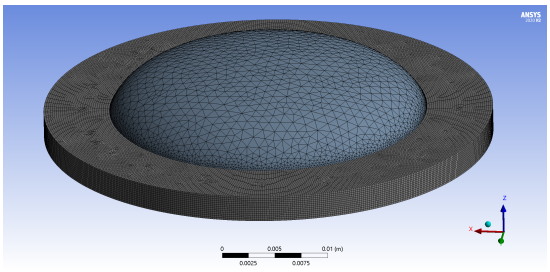

Figure 4.6: Mesh view of the engine head for test-0.

4.3.3 Test-1

For test-1, the variation applied was to the gap value. This translated into a 1 mm reduction to the dimension, from a 2.5 mm gap in test-0 to a 1.5 mm gap in test-1 while the remaining constraints stayed constant. The dimensions of the squish band for this test can be seen in table (4.2).

Table 4.2: Squish band parameters for test-1.

Gap [mm]	Angle [deg]	% of Bore Area
1.5	0	50

The complete geometry model for test-1 can be seen in figure (4.7) while the updated mesh for this variation of the engine head is represented in figure (4.8).

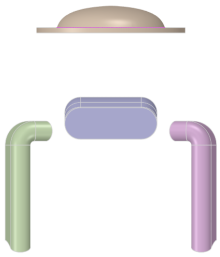

Figure 4.7: Geometry model for test-1.

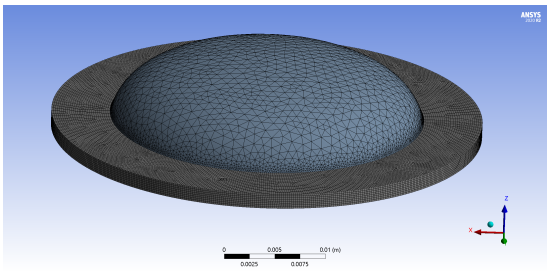

Figure 4.8: Mesh view of the engine head for test-1.

4.3.4 Test-2

For test-2 the variation implemented was having an angled squish band wall instead of a wall parallel to the piston. So, a $9.1°$ angle was introduced to squish band while the rest of the constraints from test-0 remained constant. In table (4.3) the parameters for test-2 can be seen.

Table 4.3: Squish band parameters for test-2.

Gap [mm]	Angle [deg]	% of Bore Area
2.5	9.1	50

With the changes to the squish band implemented, the final geometry model is presented in figure (4.9) and the updated mesh for the engine head in figure (4.10).

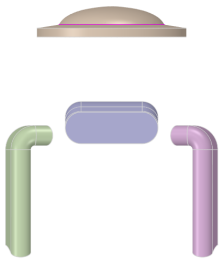

Figure 4.9: Geometry model for test-2.

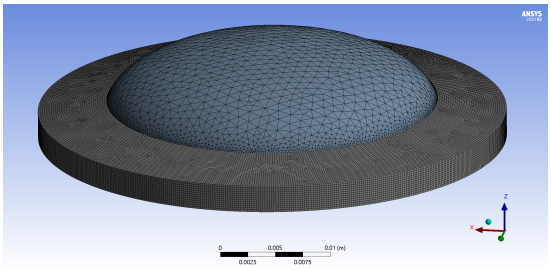

Figure 4.10: Mesh view of the engine head for test-2.

4.3.5 Test-3

For test-3, the last constraint from test-0 was adapted. This meant a variation to the percentage of the piston's bore area where a squish band is present. For this case, the dimension of the squish band was increased, from 50% (test-0) to approximately 62.75% in test-3 and, as for tests 1 and 2, the remaining constraints were kept constant. The complete parameters for this test's squish band are presented in table (4.4).

Table 4.4: Squish band parameters for test-3.

Gap [mm]	Angle [deg]	% of Bore Area
2.5	0	62.75

With the necessary modifications implemented, the complete geometry model for this simulation can be seen in figure (4.11) and the updated mesh for it's engine head in figure (4.12).

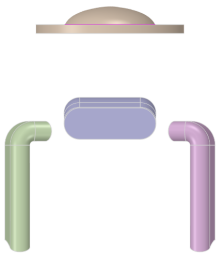

Figure 4.11: Geometry model for test-3.

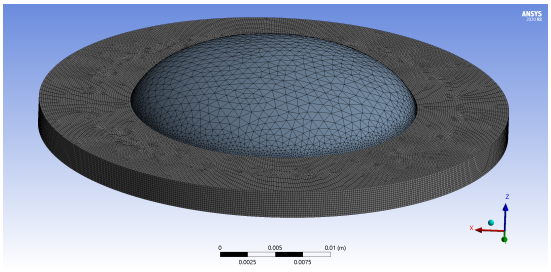

Figure 4.12: Mesh view of the engine head for test-3.

4.3.6 Test-4

Differently from the tests done before, in test-4 the objective was to vary more than one constraint of the squish band. To do this, a combination of test-1 and test-2 was done, meaning that, both the gap and the angle of the squish band was adapted. This modification translated into the parameters seen in table (4.5).

Table 4.5: Squish band parameters for test-4.

Gap [mm]	Angle [deg]	% of Bore Area
1.5	9.1	50

The complete geometry model for the simulation is presented in figure (4.13) while the updated mesh of the engine head for test-4 can be seen in figure (4.14).

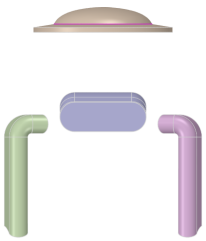

Figure 4.13: Geometry model for test-4.

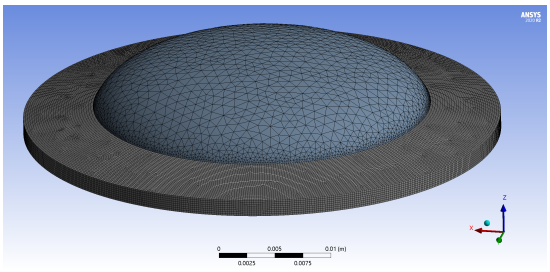

Figure 4.14: Mesh view of the engine head for test-4.

4.3.7 Test-5

For this final test, all the defined squish band constraints were varied. This meant that the gap was decreased, matching test-1, an angle was introduced, like in test-2, and the percentage of bore area occupied was increased, similarly to test-3. The complete parameters of the squish band used for this test are presented in table (4.6).

Table 4.6: Squish band parameters for test-5.

Gap [mm]	Angle [deg]	% of Bore Area
1.5	9.1	62.75

With these final modifications implemented the geometry model for test-5 is presented in figure (4.15) and the updated mesh of the engine head in figure (4.16).

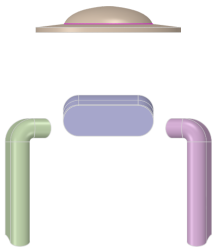

Figure 4.15: Geometry model for test-5.

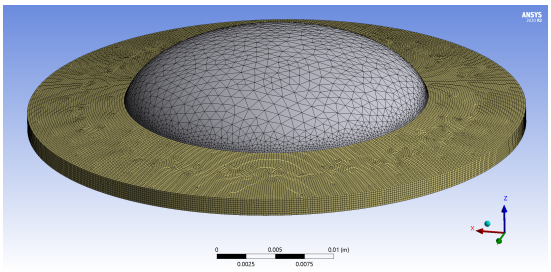

Figure 4.16: Mesh view of the engine head for test-5.

4.4 Physical Model

4.4.1 Models

The analysis was prepared in a transient state, the k-ε standard turbulence model was chosen because of the good balance between robustness and simplicity it provides while maintaining a high computational efficiency, as mentioned in section (2.3.2).

4.4.2 Species Model

Creating substance's movement, mixing and the combustion process was the next step, and for that, the species transport model was perfect, as it allows for a good simulation of multiple chemical species interaction and combustion process.

In terms of fuel, gasoline was the choice made and its reaction is shown in (4.1).

$$C_8H_{18} + 12.5O_2 + 47.02375N_2 \longrightarrow 8CO_2 + 9H_2O + 47.02375N_2 \quad (4.1)$$

From here, the mole fraction of each substance was determined from equation (4.2) in order to determine the correct inputs for the model configuration.

$$x_i = \frac{n_i}{n_{tot}} \quad (4.2)$$

Where, x_i is the mole fraction, n_i is the quantity of a determined substance and n_{tot} is the total quantity of mixture.

Since gasoline was the chosen fuel, a spark plug was required to initiate the combustion process so one was placed in the center at the top of the combustion chamber, as shown in figure (4.17). The placement was chosen in order to provide a uniform flame propagation in the chamber and improve the combustion efficiency.

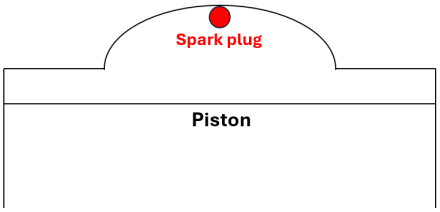

Figure 4.17: Spark plug placement

4.4.3 Boundary Conditions

For the boundary conditions of this simulation, there are two inlets, positioned at the bottom of the transfer ports, and one outlet, at the end of the exhaust port. The inlets and outlet were defined as pressure inlets and pressure outlet respectively. Fluent utilises gauge pressure in its calculations, meaning the pressure measured is relative to the atmospheric pressure as seen in equation (4.3).

$$P_{gauge} = P_{absolute} - P_{athmosferic} \quad (4.3)$$

Based on the calculations made when designing the crankcase, the expected pressure felt in the inlets would vary with the piston's movement so, for the analysis, an average value of $45000\ Pa$ was applied. For the outlet, a value of $0\ Pa$ was utilized meaning its pressure would equal the atmospheric pressure. All other boundaries of the geometry were defined as walls, with the exception of the contacts between the ports and the cylinder, which were defined as interfaces. These interfaces define locations where faces of different zones interact and the fluid must be allowed to pass. In this case, with the movement of the piston, eventually interface zones will contact and allow fluid to pass from the transfer ports into the cylinder and from the cylinder to the exhaust port.

4.4.4 Dynamic Mesh

In order to analyse the full cycle of the engine, a dynamic mesh was required, updating at every step and matching the piston's movement. ANSYS Fluent presents a tool specific for this type of mesh named in-cylinder and with it, the specifications involving the piston's movement were defined. For all cases, the engine's rpm was set to 2000, an average value in which the engine is expected to work most of the time. The step used was $0.5°$, meaning each calculation's time-step would equal a half degree of the engine's cycle, a value that would provide good results in reasonable time. Finally, the crank radius and connecting rod length were set as the values designed before, $17.54\ mm$ and $52.62\ mm$ respectively.

As mentioned before, the outer side of the cylinder's mesh was done in a layered fashion in order to allow for a good result when splitting and collapsing nodes during the mesh's movement. A value of 0.2 was defined for the collapsing and splitting factor meaning that

if the area of a node increased or decreased by 0.2 times its original size the node would split in two or merge with another node respectively. This configuration guarantees a stable mesh throughout the entire calculation and consequently good final results.
The last step is defining the motion of the different zones. There are three different types of zones that require definition:

- **Rigid Body** - Used for bodies that behave similarly to rigid-bodies, in this case the piston. Through a built-in function named "piston-full", with the specifications defined in the in-cylinder tool, the motion of the piston is created.
- **Deforming** - For the zones or faces that will suffer deformations because of the movement of the piston. This definition maintains a good mesh during the entire engine cycle.
- **Stationary** – Defines a face as motionless. Is used to maintain, faces that are adjacent to moving zones, stationary.

4.4.5 Solution Methods

The method used for the calculation was the PISO (Pressure-Implicit with Splitting of Operators) method. This is an efficient numerical algorithm used in CFD simulations to solve the Navier-Stokes equations, particularly for transient flows. It thrives specifically in transient problems, achieving convergence in fewer iterations compared to other methods by performing multiple pressure corrections in each iteration cycle this way correcting the velocity-pressure relationship more effectively and minimizing the number of iterations needed for a given time step. On top of that, it works well with almost all types of meshes and accommodates complex geometries without significant loss of accuracy. All of this makes the PISO method the most appropriate choice for the analysis.

4.4.6 Solution Controls

Under-Relaxation Factors (URF's) are numerical parameters used in iterative solvers to improve stability and convergence during the solution process. These factors control the amount by which a variable is updated during each iteration, as seen in equation (4.4) or, in other words, how much influence the result from one iteration has on the next iteration.

$$\phi^{new} = \phi^{old} + \beta \cdot (\phi^{calculated} - \phi^{old}) \quad (4.4)$$

Where, ϕ^{new} is the updated value of the variable, ϕ^{old} is the value from the previous iteration, $\phi^{calculated}$ is the new calculated value and β is the under-relaxation factor.[1]

URF values can vary between 0 and 1 and their purpose is to help prevent oscillations or divergence by smoothing changes in variables and, this way, help achieve a steady solution. For these calculations, some URF's needed to be changed from their default value. In table (4.7) the used values for the URF's can be seen.

Table 4.7: Under-relaxation factors (URF) values used.

URF	
Pressure	0.6
Density	1
Body Forces	1
Momentum	1
Turbulent Kinetic Energy	0.8
Turbulent Dissipation Rate	0.8
Turbulent Viscosity	0.8
Species	1
Energy	0.8

4.4.7 Initialization

To initialize the solution, a standard initialization was used. After that, various patches were necessary in order to properly define the different conditions in all regions. For the inlet zones, both pressure and mole fractions of C_8H_{18}, O_2 and N_2 were patched to their initial values, the same was done in the cylinder, where pressure and mole fraction of CO_2, H_2O and N_2 were patched. For the exhaust zone, only the pressure needed to be defined. The patched values are presented in table (4.8).

Table 4.8: Patched parameters after initialization.

Intake zone pressure	45 000 Pa
Exhaust zone pressure	0 Pa
Intake mole fraction of C_8H_{18}	0.01652
Intake mole fraction of O_2	0.20653
Intake mole fraction of N_2	0.77695
Cylinder mole fraction of CO_2	0.1249
Cylinder mole fraction of H_2O	0.1406
Cylinder mole fraction of N_2	0.7345
Cylinder zone pressure	2 500 000 Pa

4.4.8 Calculation Activities

In the post-processing setup, the main focus was on the combustion reaction and its components. Contour plots were generated to visualize the movement of each species. Reports of the mole fraction of each species in the cylinder as well as the rate of reaction were also created. Along with these, both contour and report plots were set to track pressure evolution throughout the simulation. All contours were updated every ten time steps, or five crank angles, and report values were saved every four time steps, or two crank angles.

Chapter 5

Results

Throughout this study, an endless number of simulations were conducted, but most of them never finished because of several different problems encountered. A great difficulty faced was managing the mesh's motion and proper contact when the ports were open, especially when just a small portion of its area was uncovered by the piston. Another great obstacle was arriving at a suitable model for the species motion and combustion process. With a complex and time-consuming analysis process, these problems became even harder to overcome because testing different approaches costed a lot of time and, on top of that, the countless software and cluster bugs encountered meant that long hours were spent until an acceptable and fully functioning analysis was achieved.

The results presented in this chapter are considered the best amongst the simulations ran for each of the test variations. Each one consisted of a total crank angle rotation of $450°$ beginning with the piston at TDC, performing a full piston cycle and ending after the exhaust port is opened for the second time. As mentioned in chapter (4.4.4) the simulations used a $0.5°$ crank angle step, so a total of 900 time steps were performed for an average of 14417 iterations and 106899.36 seconds, approximately 29 hours and 42 minutes, of total calculation time for each test.

5.1 Test-0

The purpose of this test, as stated in section (4.3), is to serve as a starting point and comparison ground to the rest of the tests that were executed.

Analysing the results from test-0, is possible to see that the engine appears to work as expected. Figures (5.1 and C.4) show that, at around 100 crank angle degrees, the ratio of CO_2 and H_2O in the cylinder begins to decrease, in line with the opening point of the exhaust port.

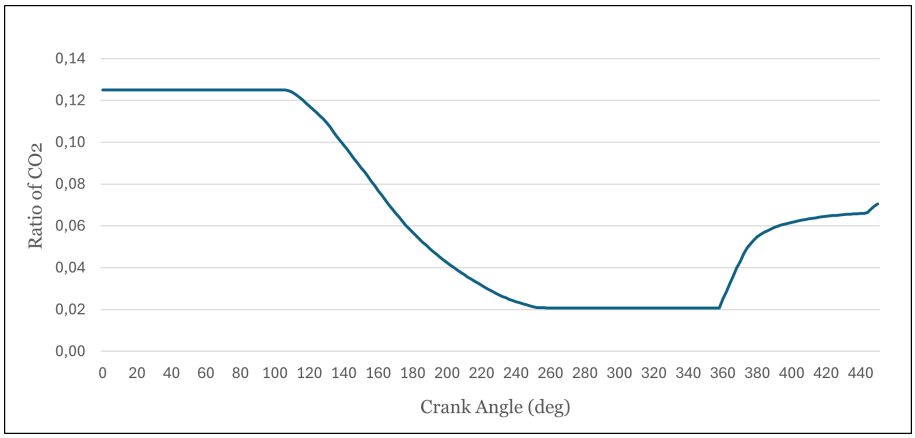

Figure 5.1: In cylinder ratio of Carbon dioxide (CO_2) in test-0.

Also, figures (5.2 and C.5) show that, at around 110° of crank angle, the ratio of C_8H_{18} and O_2 in the cylinder starts to rise, coinciding with the opening of the transfer ports. The same can be seen when analysing the contours of the ratio of C_8H_{18} presented in figures (5.3) and (5.4) where the before and after effect of the transfer ports oppening can be seen.

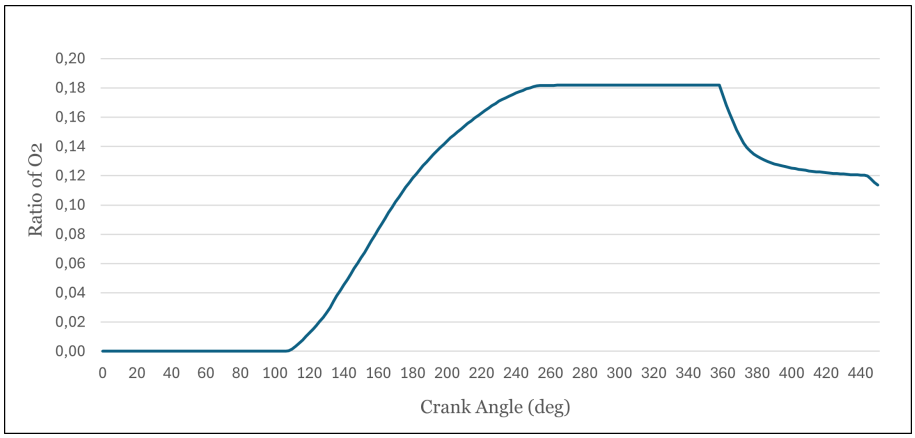

Figure 5.2: In cylinder ratio of Oxigen (O_2) in test-0.

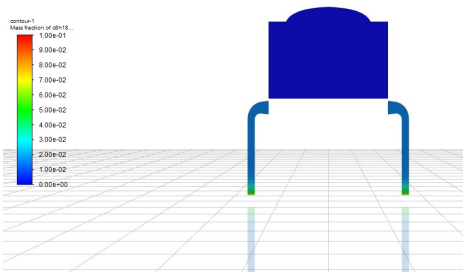

Figure 5.3: Contours of the ratio of C_8H_{18} before the opening of the transfer port (100°) in test-0.

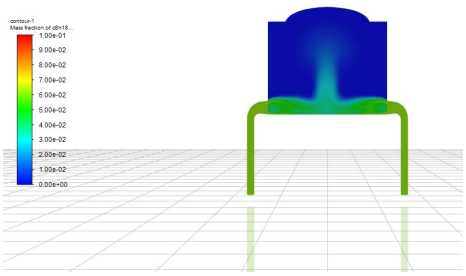

Figure 5.4: Contours of the ratio of C_8H_{18} after the opening of the transfer port (125°) in test-0.

After 240° of crank angle, all ports are closed and, because of that, the ratio of all species stabilizes. Near 360° of crank angle when the piston is close to TDC, the spark plug ignites and variations can be seen in the ratio of all species, meaning the reaction process is taking place. The same can be seen in both the values in figure (5.9) and the contours in figures (5.5, 5.6, 5.7 and 5.8) of the rate of reaction.

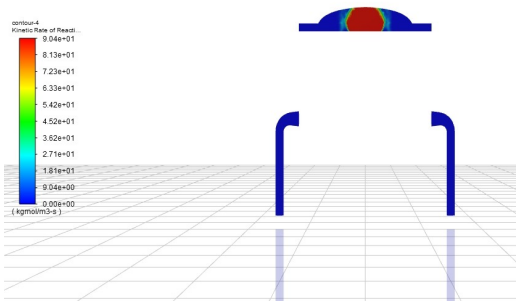

Figure 5.5: Contours of the rate of reaction at (360°) in test-0.

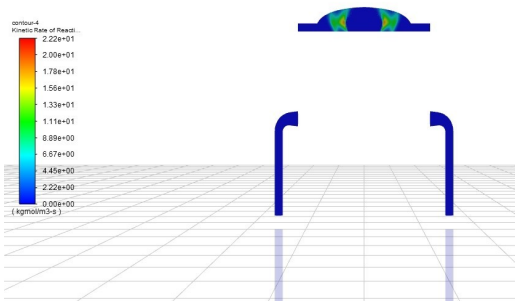

Figure 5.6: Contours of the rate of reaction at (365°) in test-0.

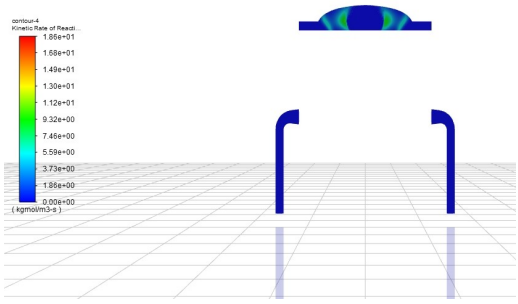

Figure 5.7: Contours of the rate of reaction at (370°) in test-0.

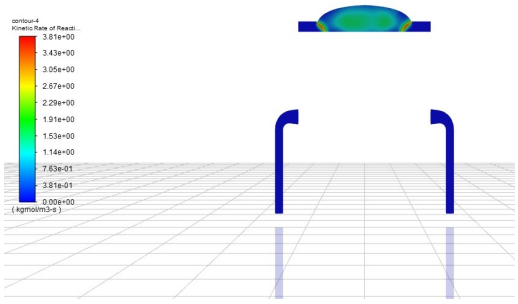

Figure 5.8: Contours of the rate of reaction at (375°) in test-0.

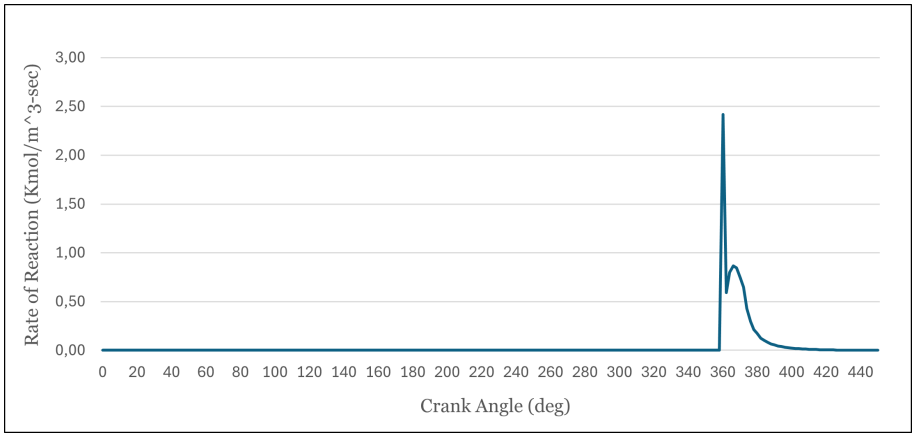

Figure 5.9: Rate of Reaction in test-0.

Finally, figure (5.10) provides the value for peak pressure, that occurs when the piston is near TDC and the combustion process is taking place, in this case, approximately $3\,353\,976\ Pa$.

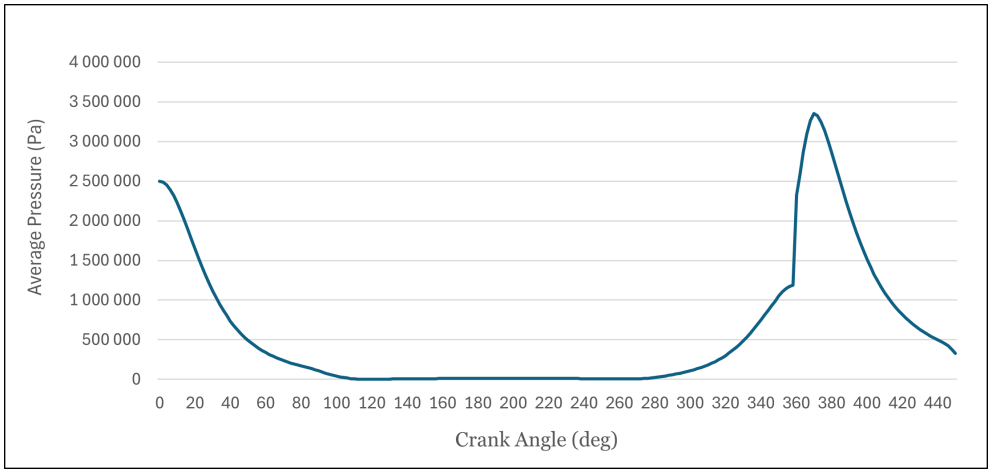

Figure 5.10: In cylinder pressure in test-0.

5.2 Test-1

In test-1, the gap between the squish band and the piston was reduced from 2.5 mm (test-0) to 1.5 mm. Analysing the results, it is clear that although the graphs behave similarly, the values obtained indicate an increased combustion efficiency. Figure (5.11) shows that the ratio of O_2 in the cylinder after combustion is lower than the one in test-0, figure (5.2), which indicates an improved reaction. This is verified when analysing figure (5.12) which confirms a higher value of the rate of reaction, in comparison to the one seen in the base test, figure (5.9).

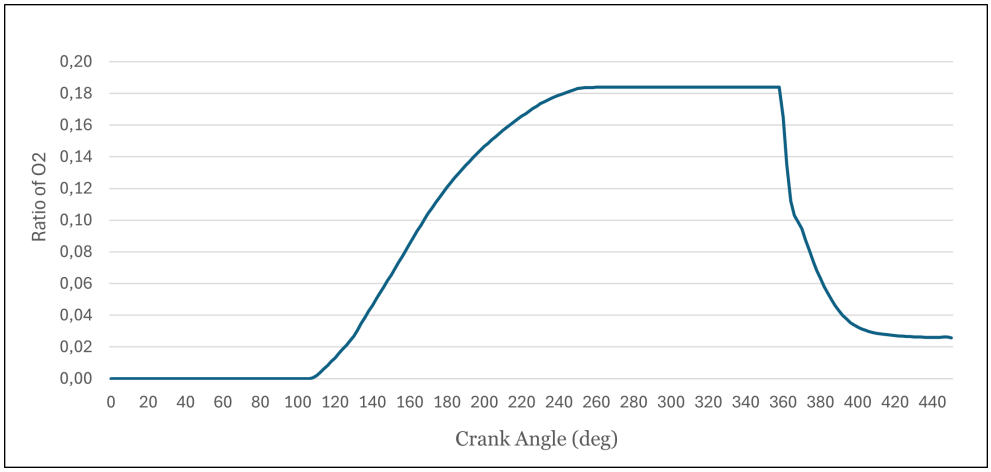

Figure 5.11: In cylinder ratio of Oxigen (O_2) in test-1.

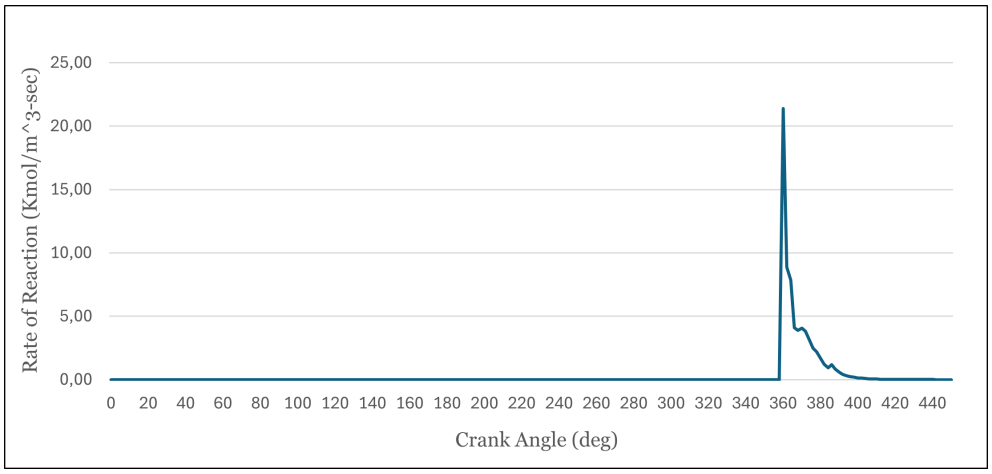

Figure 5.12: Rate of Reaction in test-1.

When evaluating the pressure, figure (5.13), an increased value of peak pressure can be seen comparing to the one in test-0, this means that this configuration will impose greater stress on the cylinder and piston walls which can, in the long run, reduce component lifetime.

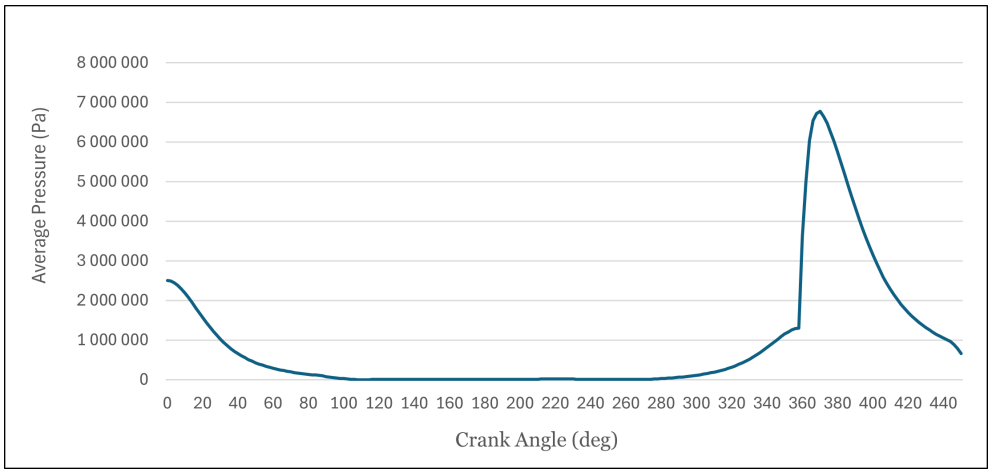

Figure 5.13: In cylinder pressure in test-1.

5.3 Test-2

For test-2, an angle was introduced to the squish band. Analysing the results, in figures (5.14) and (5.15) it is possible to see an improvement in combustion efficiency from test-0, although not as big as the one seen in test-1.

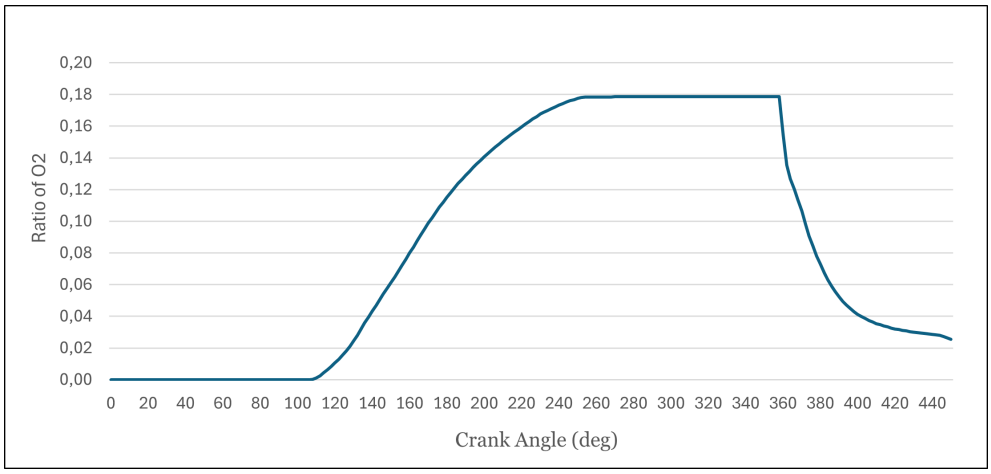

Figure 5.14: In cylinder ratio of Oxigen (O_2) in test-2.

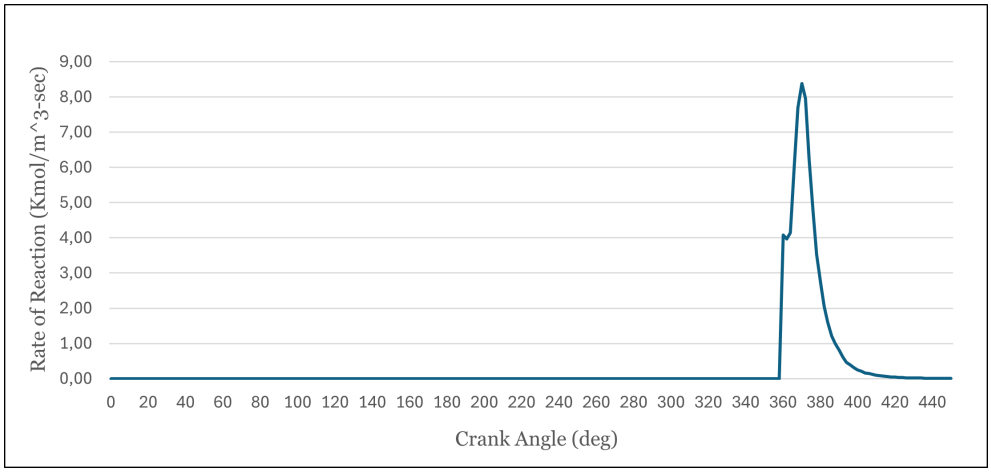

Figure 5.15: Rate of Reaction in test-2.

Similarly, in figure (5.16), the peak value of pressure in the cylinder increases comparing to the one seen in test-0 but not as much as it had increased in test-1.

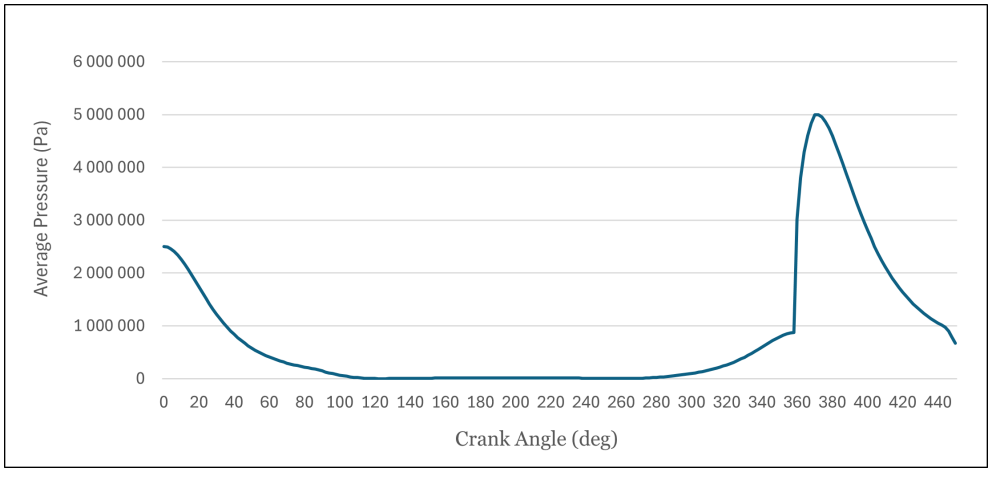

Figure 5.16: In cylinder pressure in test-2.

From the results of test-2, it is possible to conclude that although an angled squish band will improve the engine's combustion efficiency, the effect is not as considerable as the one seen when reducing the gap (test-1). One detail noticed after analysing the results is that the addition of the angle will increase the gap in portions of the squish band, so, a new test where an angle is introduced and the gap is reduced will be performed.

5.4 Test-3

For test-3, the piston's bore area affected by a squish band was increased, effectively amplifying the effect of the squish band. When analysing figures (5.17) and (5.18) an improved combustion can be seen compared to the base test (test-0) both by the higher peak in rate of reaction and the reduced value of the ratio of O_2 left after combustion.

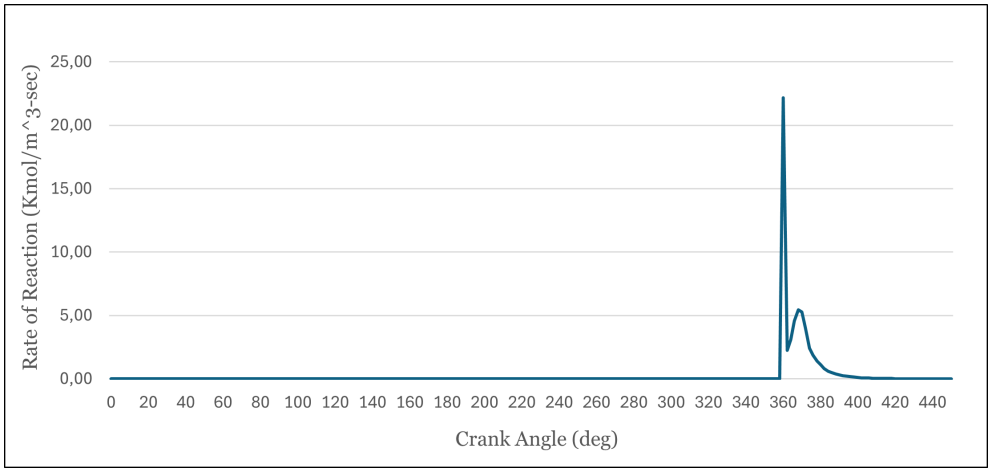

Figure 5.17: Rate of Reaction in test-3.

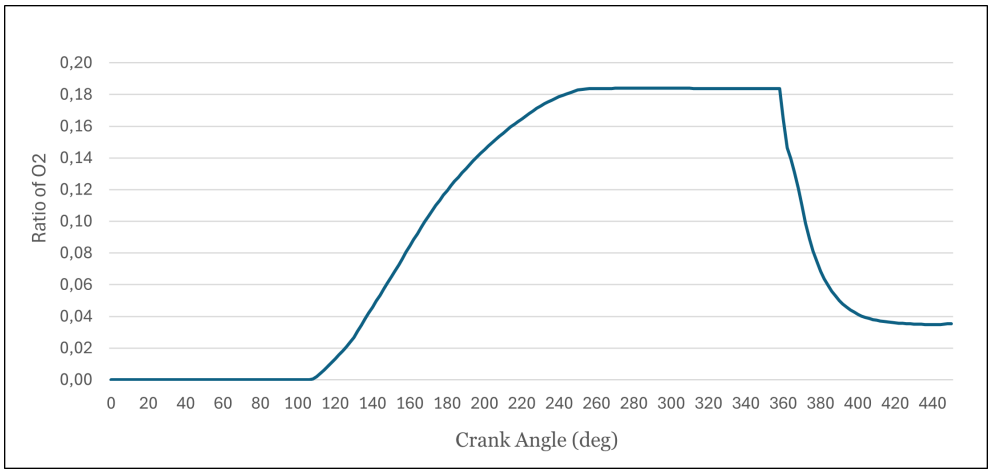

Figure 5.18: In cylinder ratio of Oxigen (O_2) in test-3.

Although, the ratio seen in figure (5.18) has a value close to 0.04 while in tests 1 and 2 the value was close to 0.02. This difference can probably be explained by the fact that some fresh mixture can be trapped under a wider squish band, which is the case for test-3, and prevented from being combusted. This was confirmed while analysing the contours of the mass fraction of C_8H_{18} in the cylinder, which can be seen in figure (5.19), where, at 385º of crank angle, it is possible to see some fresh mixture trapped in the corners of the squish band.

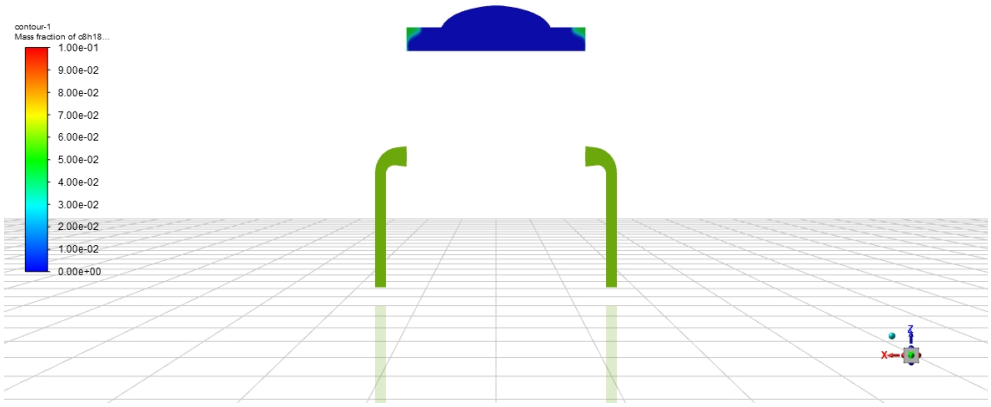

Figure 5.19: Contours of mass fraction of C_8H_{18} at 385º crank angle for test-3.

5.5 Test-4

This test was prepared in order to analyse the effects of an angled squish band with a smaller gap, as previously mentioned. From figures (5.20) and (5.21) an improvement of combustion efficiency can be seen when comparing to all the previously conducted tests.

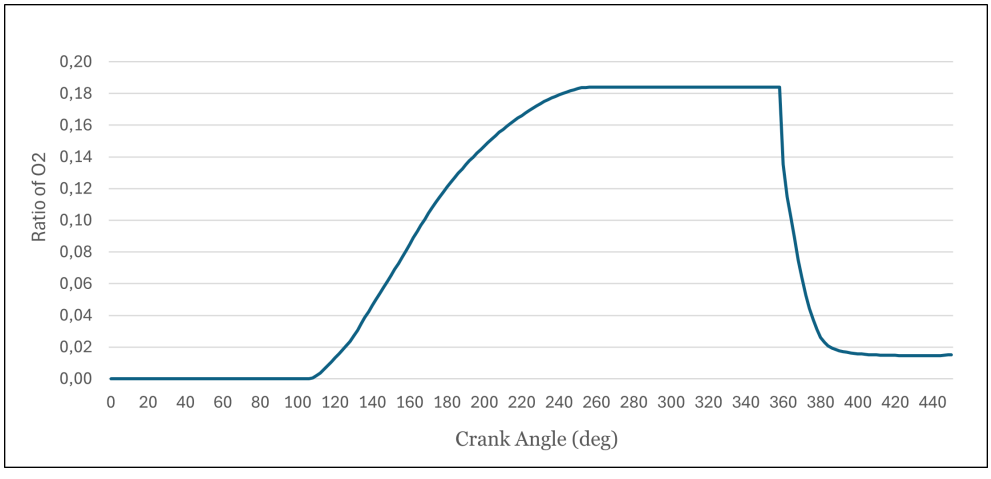

Figure 5.20: In cylinder ratio of Oxigen (O_2) in test-4.

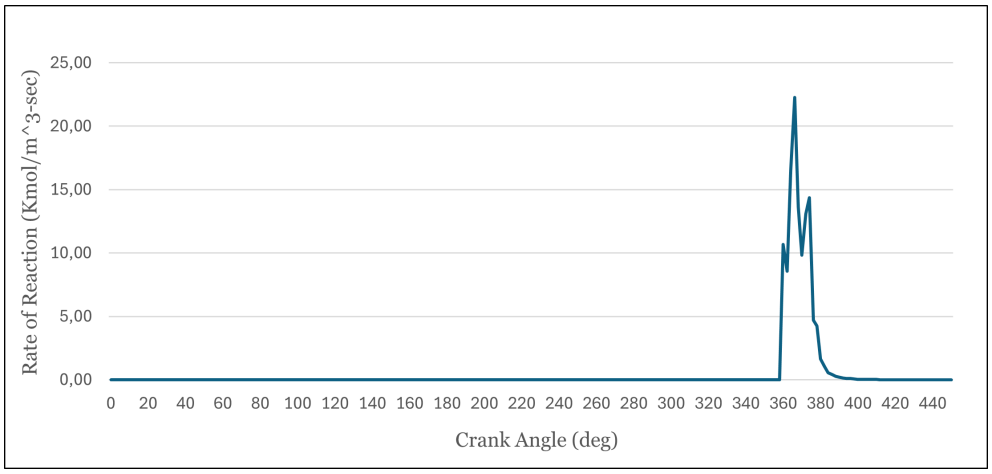

Figure 5.21: Rate of Reaction in test-4.

Especially comparing to test-1, figure (5.12), and test-2, figure (5.15), the improvement in rate of reaction and combustion time is considerable while the peak pressure value, seen in figure (5.22), has only slightly increased from the ones seen in figures (5.13) and (5.16). This concludes that, a combination of this two constrain variations of the squish band is likely to be an improvement over having just one or the other.

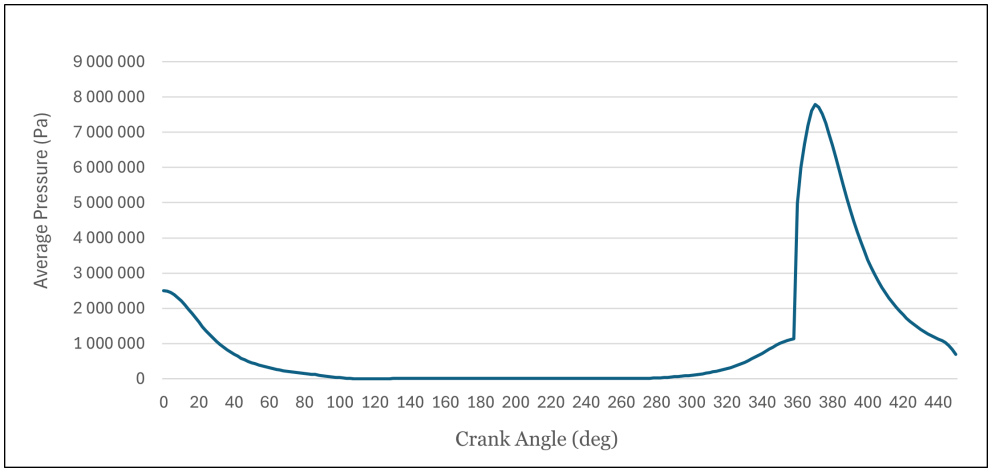

Figure 5.22: In cylinder pressure in test-4.

5.6 Test-5

For the final test (test-5), all the previous configurations were merged and analysed together and the results show an improvement on all the previous calculations. In terms of the rate of reaction, figure (5.23), this test delivered the greatest peak and at the same time the fastest reaction, finishing combustion at around 380 crank angle degrees.

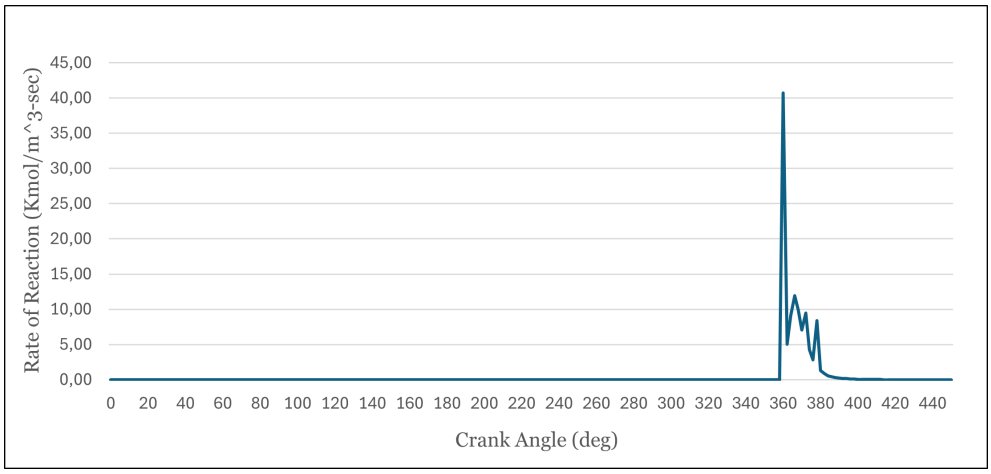

Figure 5.23: Rate of Reaction in test-5.

The problem experienced in test-3 where, with a wider squish band, some mixture got trapped in the corners and was lost, appears to no longer be so impactful in test-5. With the same percentage of bore's area as test-3, but with the addition of an angled squish band, the ratio of O_2 in the cylinder after combustion, which can be seen in figure (5.24), was reduced compared to the one in test-3, figure (5.18).

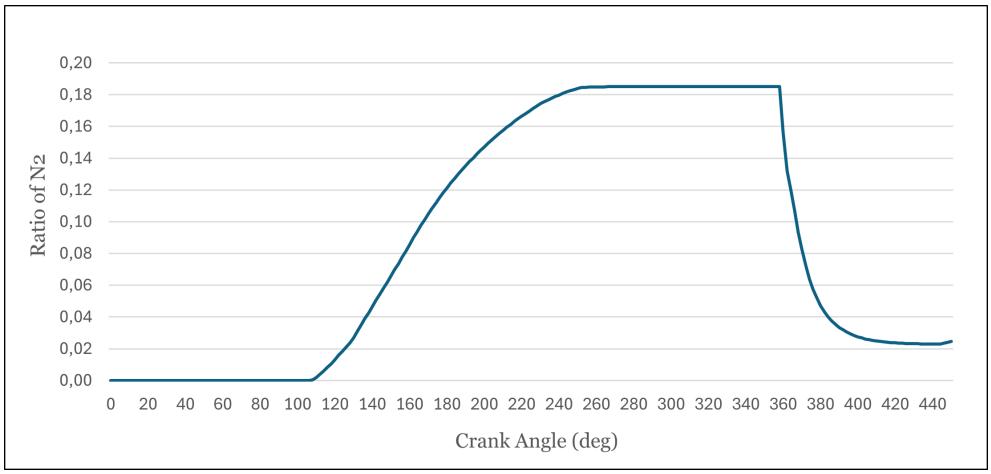

Figure 5.24: In cylinder ratio of Oxigen (O_2) in test-5.

The same conclusion can be reached when analysing the contours of the mass fraction of C_8H_{18}, figure (5.25), where, for the same crank angle (385°) the amount of fresh mixture lost in the corners is significantly less compared to the one seen in test-3, figure (5.19).

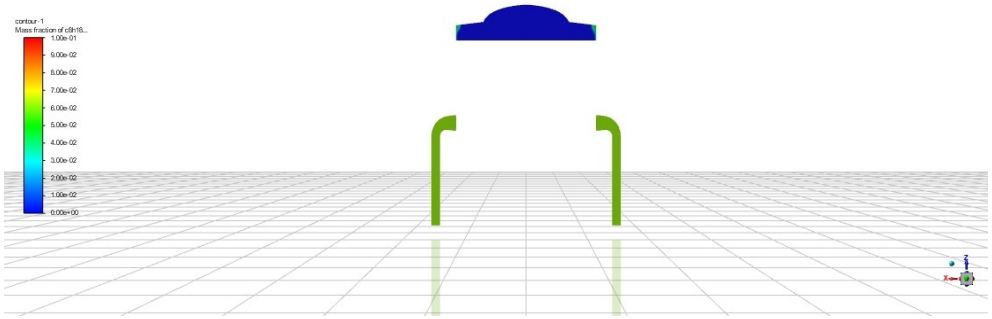

Figure 5.25: Contours of mass fraction of C_8H_{18} at 385º crank angle for test-5.

Finally, examining the pressure measurement, figure (5.26), the peak value appears to stay consistent with the previous test without any significant increases. However, compared to the base test (test-0), there is a considerable raise in the peak pressure felt in the cylinder. This high pressure is a notable downside of this test's configuration and worth noting as it will lead to a greater mechanical stress on the engine's components, higher temperatures and an increased risk of component failure.

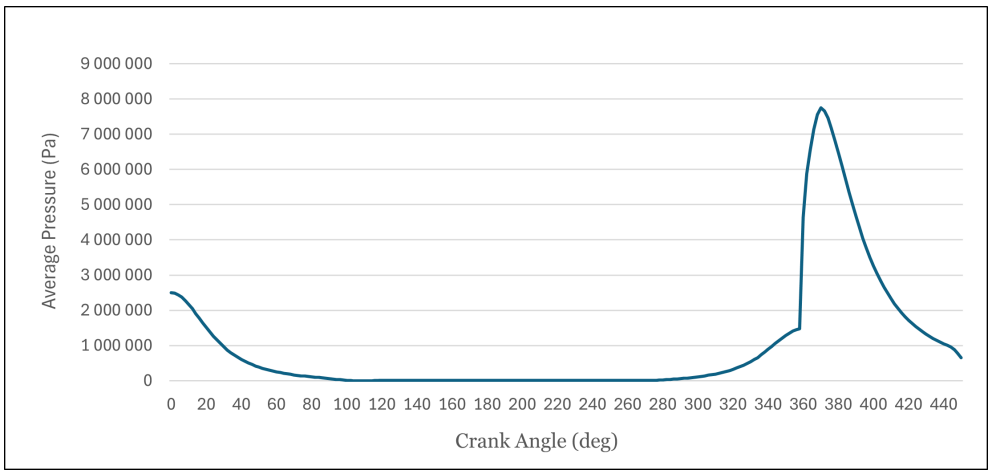

Figure 5.26: In cylinder pressure in test-5.

5.7 Final impressions

Overlooking the results of all six variations calculated there are several considerations to be made. In general, the results indicate that the reduction of the gap, the introduction of an angle and the increase of percentage of bore's area of a squish band in a two-stroke piston ported engine will likely lead to an increase in combustion performance, as confirmed in figure (5.27) where the values of the rate of reaction for all six tests are graphed. In it, every new variation produces an increased peak rate of reaction and, at the same time, a reduced combustion time. Even more, the combination of variations, seen in test-4 and 5, leads to an even higher rate of reaction and smaller combustion time.

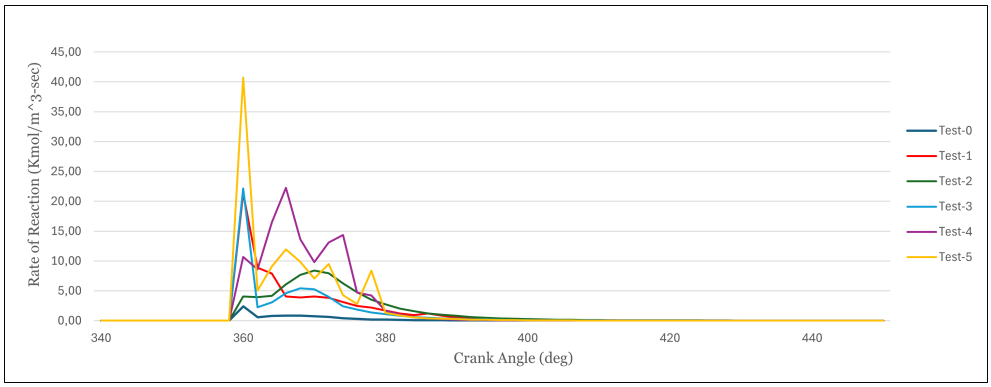

Figure 5.27: Rate of reaction for all tests.

On the other hand, when looking at the pressure values of all six tests, figure (5.28), it is obvious that every variation eventually leads to an increased peak value of pressure. To ensure that an engine is capable of supporting higher pressures will require a more complex structure and additional manufacturing costs which may be an obstacle.

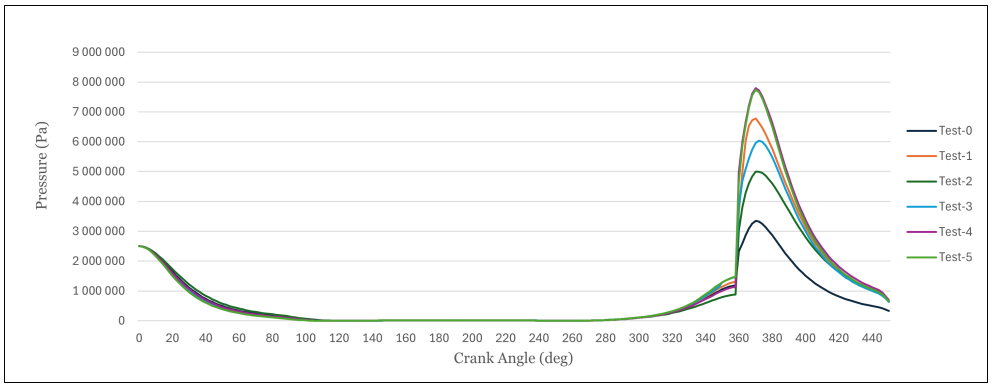

Figure 5.28: In cylinder pressure for all tests.

Additionally, as seen in tests 3 and 5, increasing the percentage of bore's area brings an additional problem because, a wide enough squish band, will eventually trap more fresh mixture in it's corners leading to fuel losses and a higher specific fuel consumption. The introduction of an angled squish band provides a good mitigation of this problem, as seen in test-5, and so, for wider squish band's the addition of an angle becomes even more important.

Chapter 6

Final considerations

This dissertation presents the analysis of the influence of the squish band on a two-stroke SI piston ported engine. The engine in study was designed and dimensioned from scratch, as well as the different engine heads utilized for every test variation. The CAD was made utilizing the CATIA V5 software and the numerical analysis was performed in ANSYS Fluent.

For the dimensioning process of the base engine design, the objective was a 50cc small utility based two-stroke piston ported engine. The different squish band models to be tested were designed with three different parameter variations: the gap between the squish band and the piston crown at TDC, the angle of the squish band and the percentage of the piston's bore area where the squish band was present.

Considering the CFD analysis, the simulations ran on the multi-core high performance cluster of Universidade da Beira Interior and after countless missed calculations due to bugs, errors and improper definitions a suitable model for the engine's cycle and species movement and combustion was achieved. With the appropriate configuration, the simulation was repeated for the six different test variations and the results were presented and analysed. Regarding the results, the conclusion was that, every variation tried, provided an improved combustion efficiency when compared to the base test. When multiple constrains were varied simultaneously the results revealed an even better combustion process. One important detail analysed was that for wide enough squish bands the fresh mixture will get trapped in the corners below them and, in those cases, an angled squish band must be implemented to help prevent fuel losses and improve the engine's specific fuel consumption. With the improved combustion efficiency that came with every test, also a greater peak value of pressure was felt in the cylinder. This increased pressure would cause higher stress in the engine's components increasing wear and reducing their lifespan. Also, the lubrication demand will be higher and increased noise and vibrations might also be a problem. Overall, the improved performance will come at a cost of making a slightly more complex and costly engine.

This analysis was a long and challenging work that in the end turned out to be quite rewarding. The knowledge gained on internal combustion engines, the designing and dimensioning process and, specially, on CFD simulation and software's is immeasurable and the results were very fulfilling.

6.1 Future Works

The simulation carried in this study was very theoretical and many real-world aspects were not considered for this analysis. With that in mind, this work can evolve by, for example:

- Utilizing models that are more time and computational demanding but provide more precise results, especially turbulence and combustion models.
- Improve the utilized mesh quality for more exact results, again at a cost of time and computational resources.
- Simulate the engine's combustion including the incomplete combustion products in order to track the engine's emissions.
- Implement an additional test where the squish band is angled, similarly to test-2, but with a curved piston crown that would maintain a consistent gap through the entire squish band.
- Experimental studies of the squish band's influence on the engine's combustion performance could also be a valuable next step.

Bibliography

[1] ANSYS. *Fluent Theory Guide*. ANSYS, Inc., 2009. 41

[2] A. Graham Bell. *Two-Stroke Performance Tuning in Theory and Practice*. J.H. Haynes and Co Ltd, 1983. 8, 9, 13, 15

[3] Gordon P. Blair. *Design and Simulation of Two-Stroke Engines*. Society of Automotive Engineers, Inc., 1996. 3

[4] J. Blazek. *Computational Fluid Dynamics: Principles and Applications*. ELSEVIER, 2001. 17, 19

[5] John B.LHeywood. *Internal Combustion Engine Fundamentals*. McGraw-Hill, Inc, 1988. 6, 7, 8, 11, 12

[6] Colin R. Ferguson and Allan T. Kirkpatrick. *Internal Combustion Engines: Applied Thermosciences, Third Edition*. John Wiley & Sons Ltd, 2016. 4, 15

[7] Michael Forrest. Available at `https://www.dragonfly75.com/moto/SquishVelocity.html`. Accessed: 4/2025. 9

[8] Marty's Garage. Available at `https://martysgarage.info/reference/two-stroke-port-duration/`. Accessed: 08/2024. 13

[9] Gordon Jennings. *Two-stroke tuner's handbook*. H.P.Books, 1973. 9, 10, 11, 14, 26, 29, 35

[10] Jr. John D. Anderson. *Computational Fluid Dynamics: The Basics with Applications*. McGraw-Hill, Inc., 1995. 17, 18, 21

[11] Cer Motor. Available at `https://cermotor.com.pl/en/guides/engine-blocks/`. Accessed: 12/2024. 4

[12] Atrac Engine Parts. Available at `https://www.atracparts.com/blog/everything-about-piston-ring-types-their-functions-and-material-used-ultimate-gui` Accessed: 12/2024. 7

[13] Stephen B. Pope. *Turbulent Flows*. Cambridge: Cambridge University Press, 2000. 23

[14] Powercdi. Available at `https://www.powercdi.com/manual/combustion/squish/en.html`. Accessed: 12/2024. 1

[15] Willard W. Pulkrabek. *Engineering Fundamentals of the Internal Combustion Engine*. Prentice Hall, 2004. 7, 8, 11

[16] SAVREE. Encyclopedia. Available at `https://savree.com/en/encyclopedia/engine-crankshaft`. Accessed: 09/2024. 11

[17] Hotshot Secret. Available at https://www.hotshotsecret.com/two-stroke-vs-four-stroke-engines/. Accessed: 11/2024. 3

[18] Prime Source. Available at https://primesourceco.com/latest-news/what-are-the-different-parts-of-a-2-stroke-engine/. Accessed: 11/2024. 3

[19] Richard Stone. *Introduction to internal combustion engines*, volume 3. The MacMillan Press LTD, 1999. 5, 6, 14

[20] VCalc. Available at https://www.vcalc.com/wiki/EmilyB/Position+of+the+piston+of+engine+with+respect+to+crank+angle. Accessed: 06/2024. 28

Appendix A

Dimensioning

A.1 Engine model-CAD

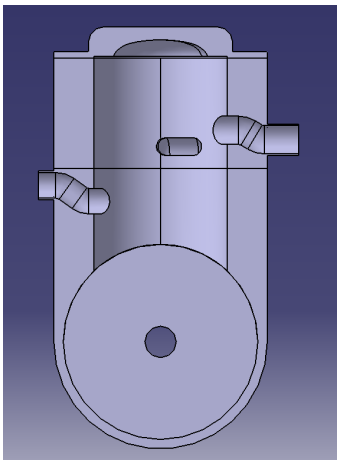

Figure A.1: Engine's cylinder and crankcase design

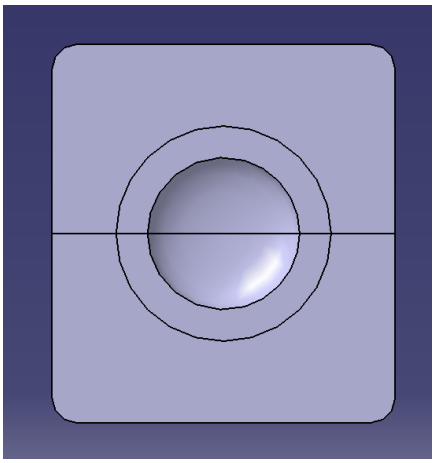

Figure A.2: Bottom view of the engine head design

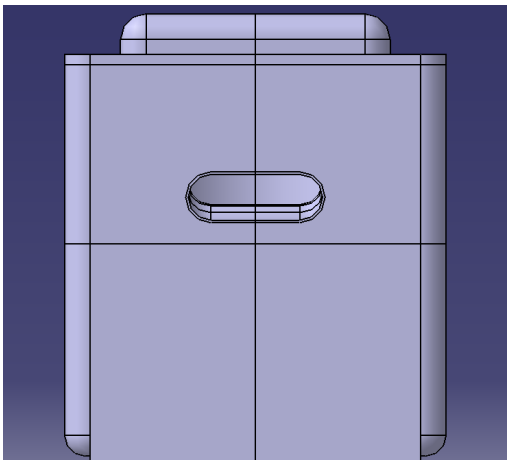

Figure A.3: Exhaust side view

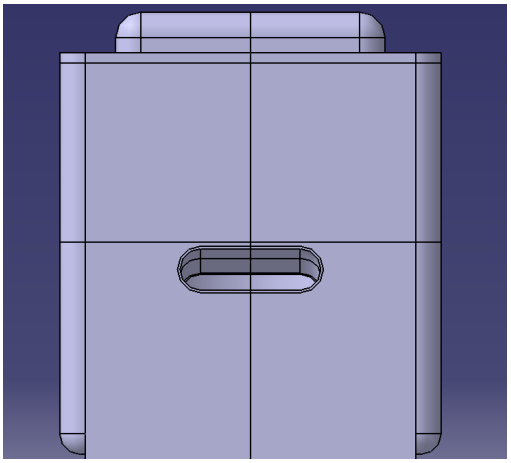

Figure A.4: Intake side view

Appendix B

Simulation

B.1 Mesh

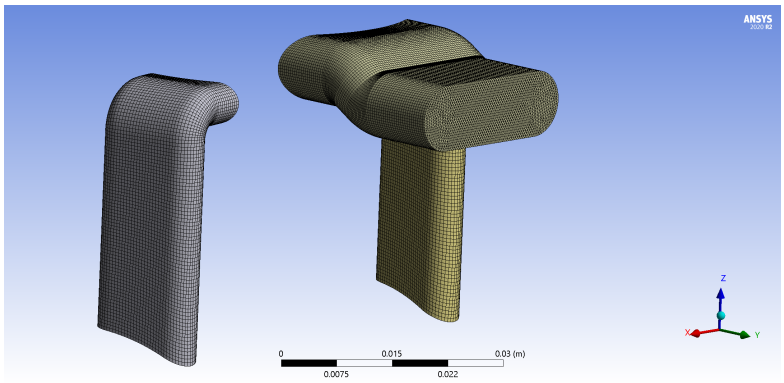

Figure B.1: Mesh view of the exhaust port.

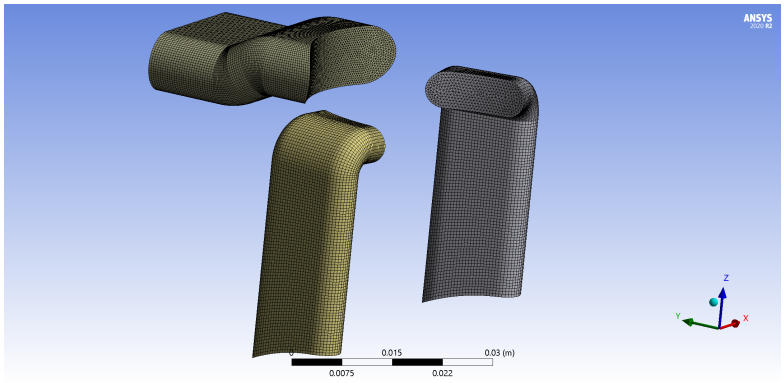

Figure B.2: Mesh view of the transfer ports.

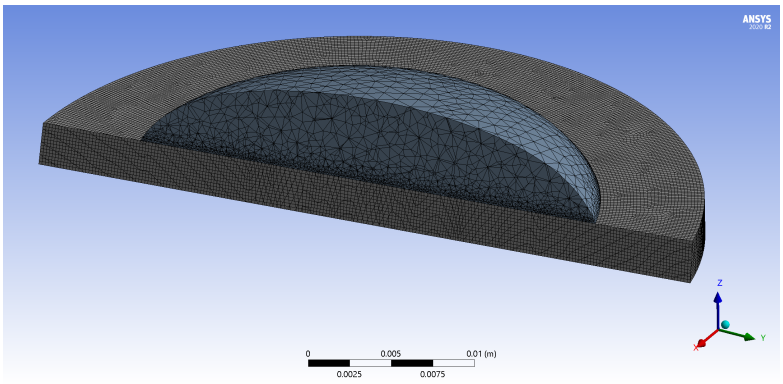

Figure B.3: Section view of the mesh for test-0.

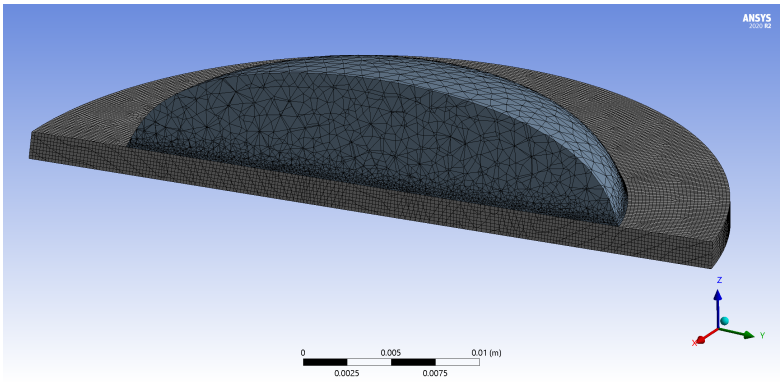

Figure B.4: Section view of the engine head's mesh for test-1.

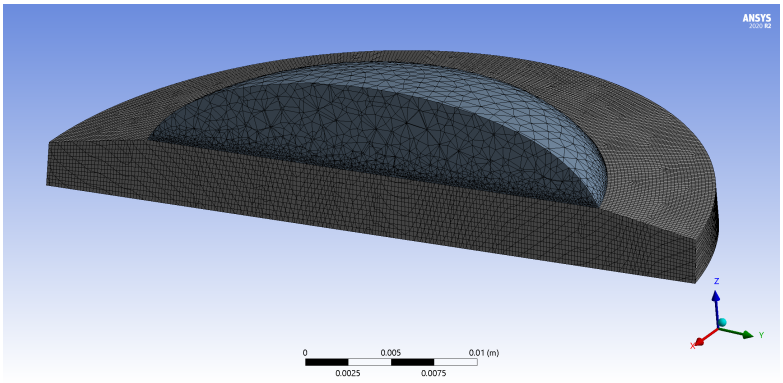

Figure B.5: Section view of the engine head's mesh for test-2.

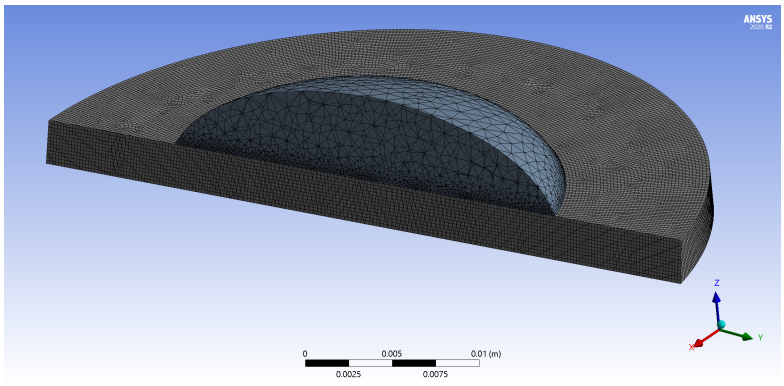

Figure B.6: Section view of the engine head's mesh for test-3.

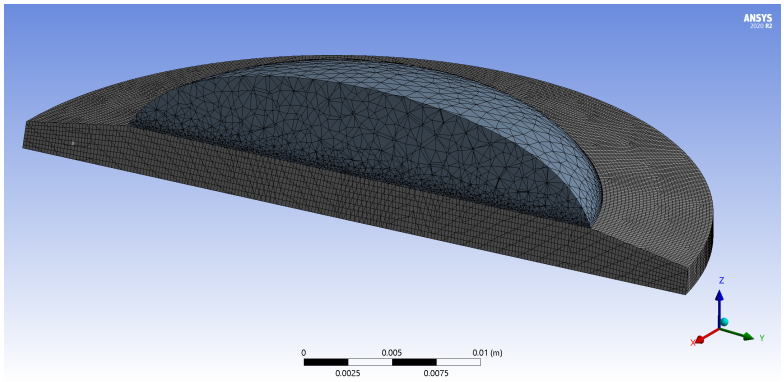

Figure B.7: Section view of the engine head's mesh for test-4.

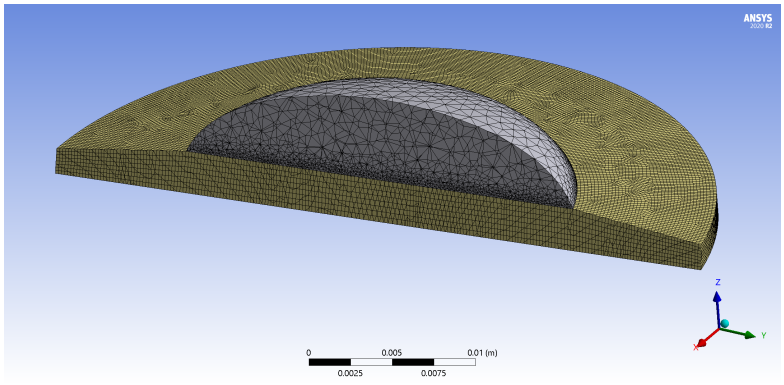

Figure B.8: Section view of the engine head's mesh for test-5.

Table B.1: Parameters of the engine ports mesh.

Method	Multizone
Mapped mesh type	Prism
Free mesh type	Not allowed
Face meshing	Active in interfaces
Face mesh mapped	Yes
Transfer ports element size	0.5 mm
Exhaust port element size	0.4 mm
Behavior	Soft
Growth rate	1.2

Table B.2: Parameters of the engine cylinder mesh.

Mesh method in cylinder	Multizone
Mapped mesh type	Hexa/Prism
Surface mesh type	Pave
Free mesh type	Not allowed
Cylinder element size	0.2 mm
Mesh method in chamber	Free mesh
Chamber element size	1 mm
Behavior	Soft
Growth rate	1.2
Contact sizing	Active in interface zones
Contact sizing type	Element size

Appendix C

Results

C.1 Test-0

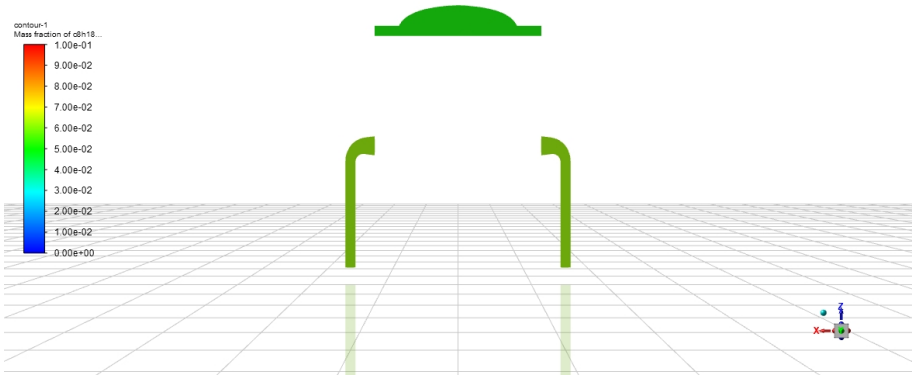

Figure C.1: Contours of the ratio of C_8H_{18} at (355°).

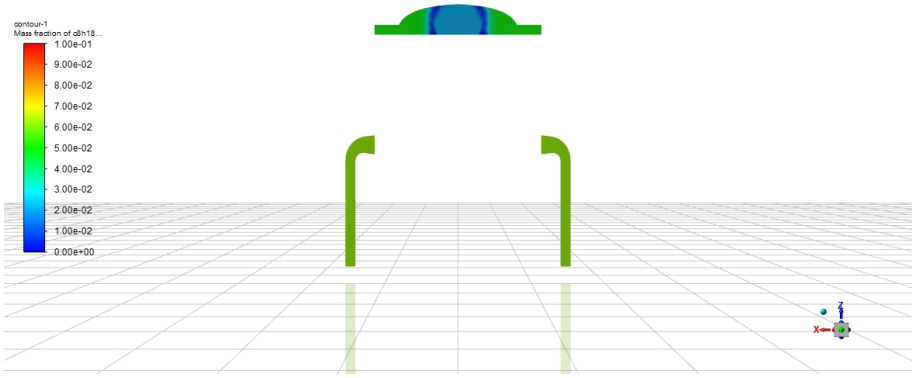

Figure C.2: Contours of the ratio of C_8H_{18} at (360°).

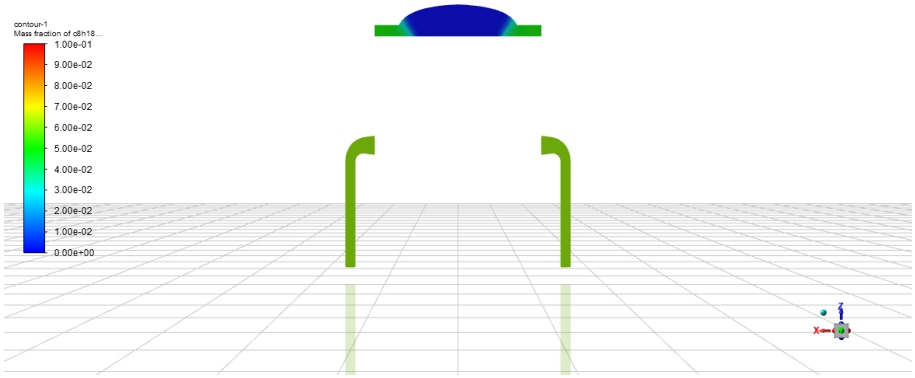

Figure C.3: Contours of the ratio of C_8H_{18} at (370°).

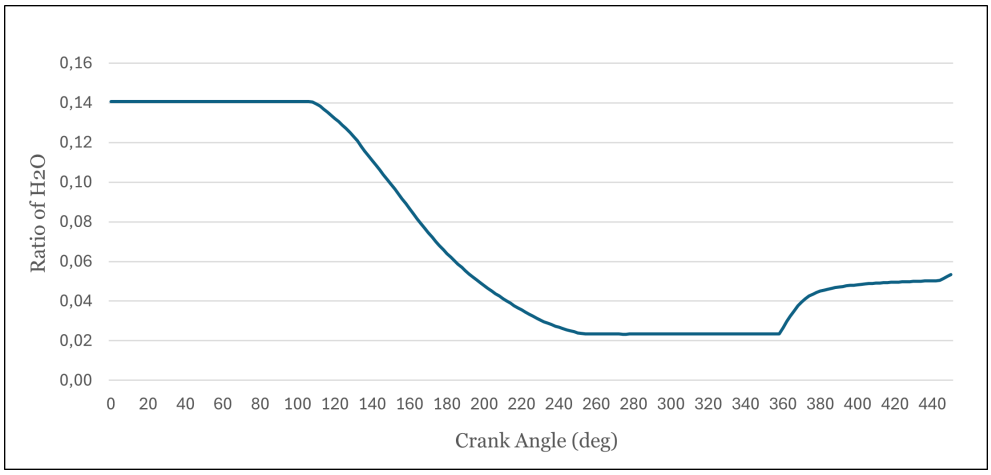

Figure C.4: In cylinder ratio of water vapor (H_2O) in test-0.

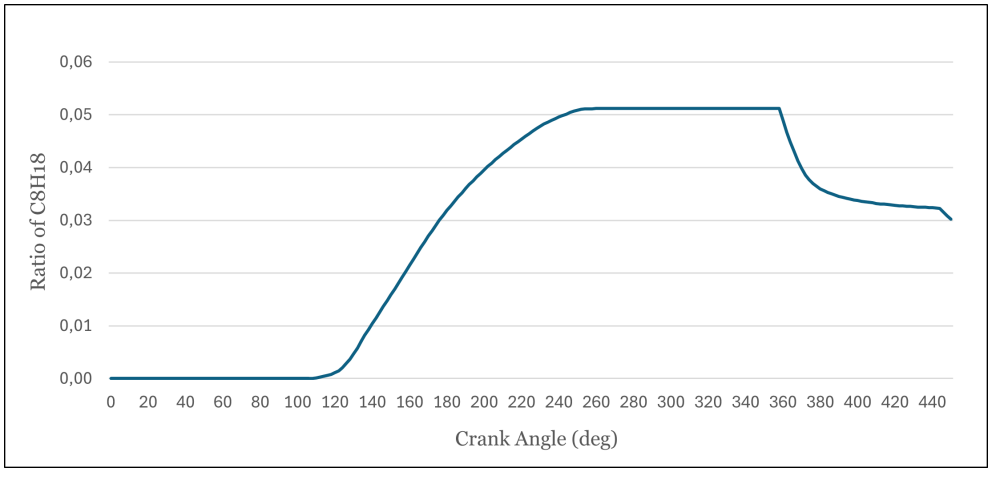

Figure C.5: In cylinder ratio of octane (C_8H_{18}) in test-0.

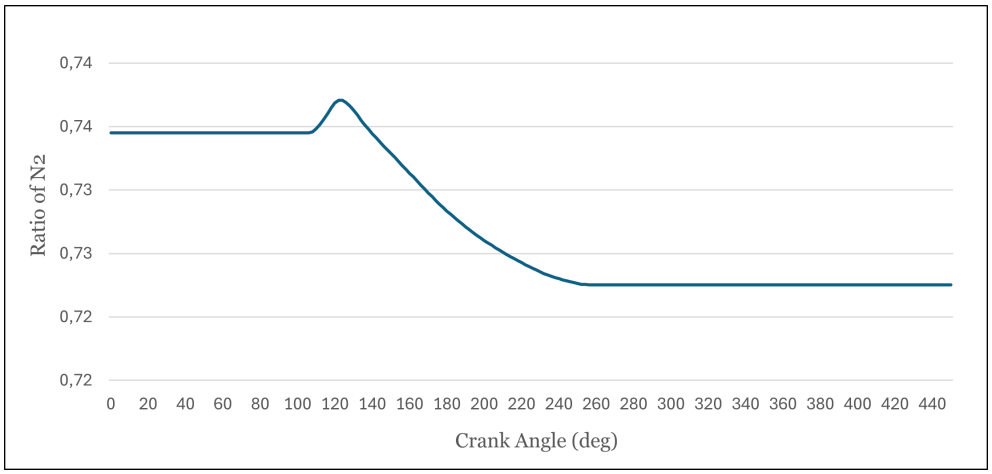

Figure C.6: In cylinder ratio of nitrogen (N_2) in test-0.

C.2 Test-1

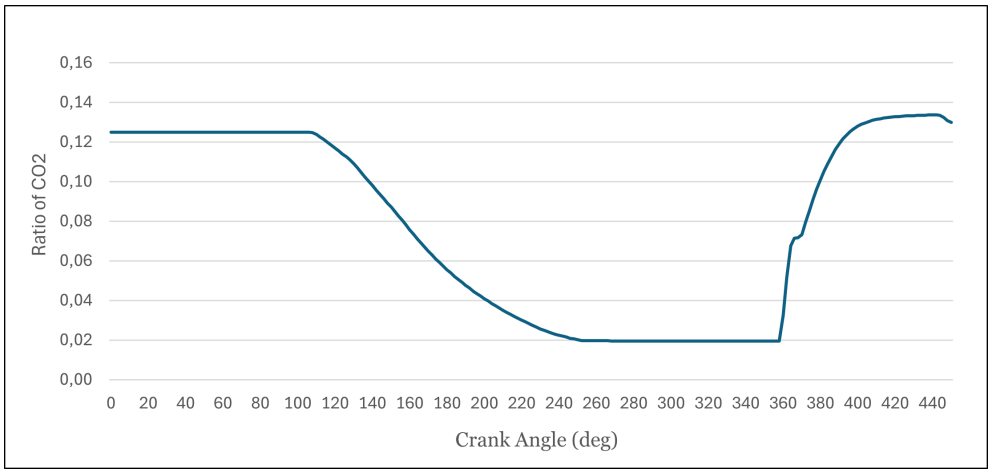

Figure C.7: In cylinder ratio of Carbon dioxide (CO_2) in test-1.

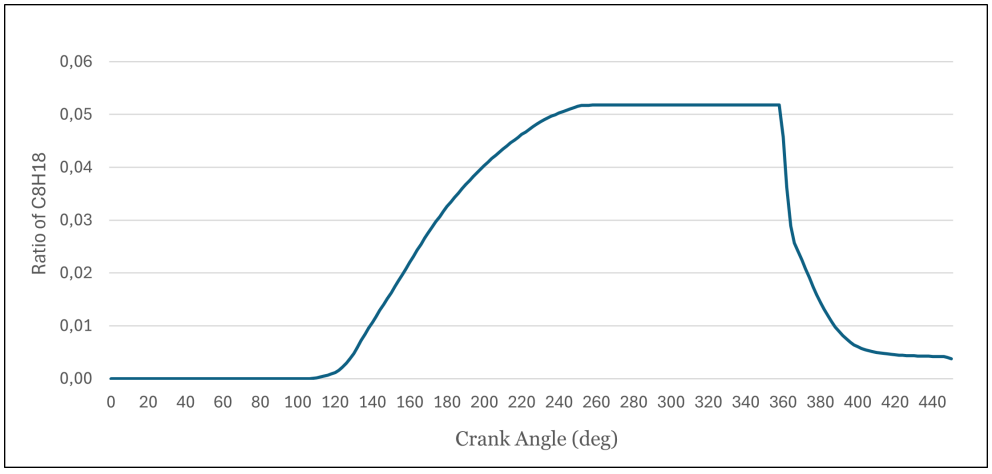

Figure C.8: In cylinder ratio of octane (C_8H_{18}) in test-1.

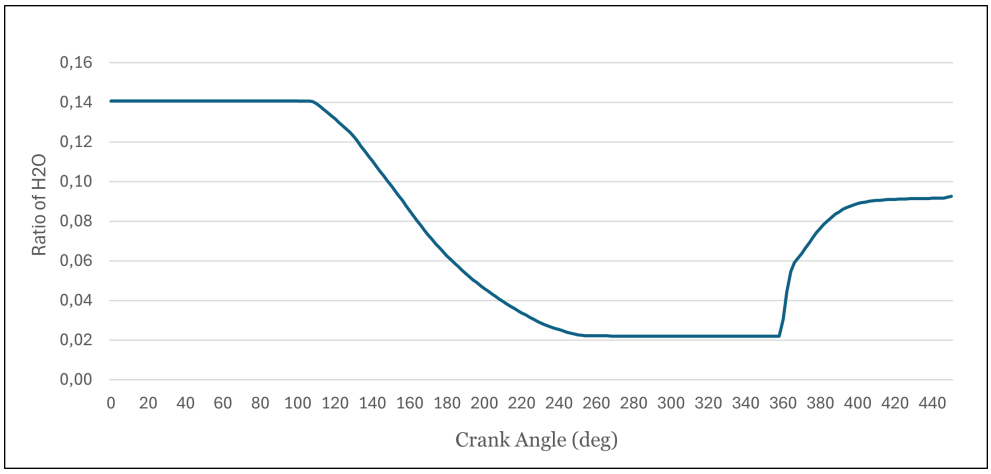

Figure C.9: In cylinder ratio of water vapor (H_2O) in test-1.

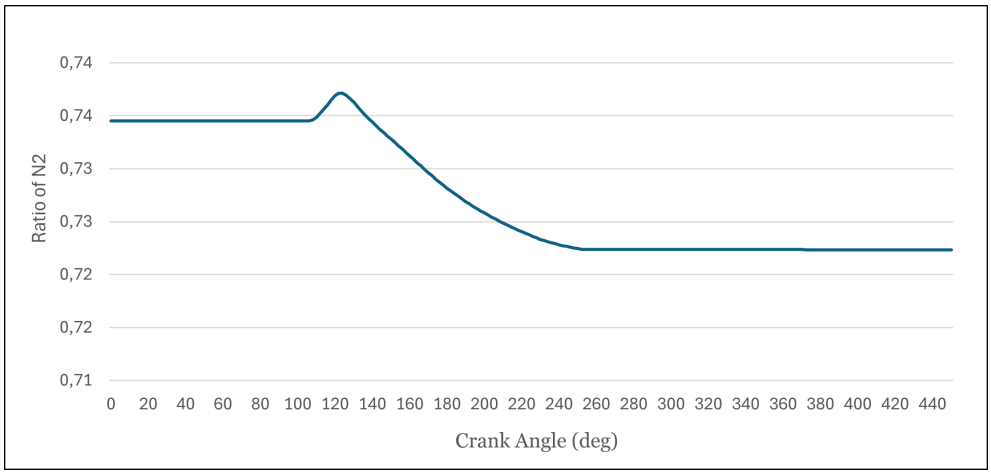

Figure C.10: In cylinder ratio of nitrogen (N_2) in test-1.

C.3 Test-2

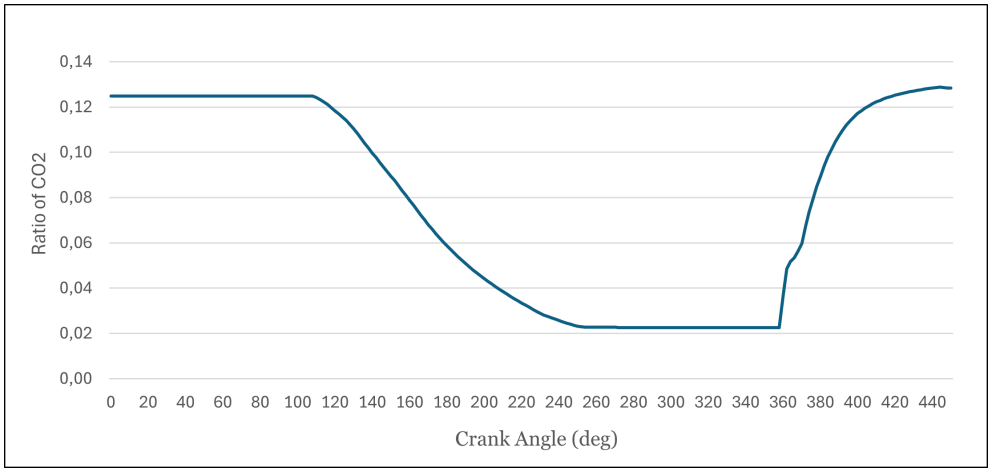

Figure C.11: In cylinder ratio of Carbon dioxide (CO_2) in test-2.

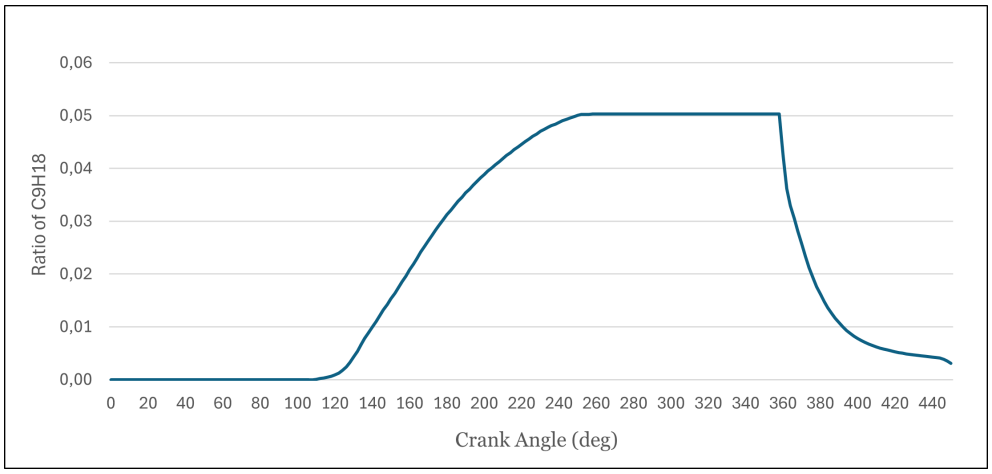

Figure C.12: In cylinder ratio of octane (C_8H_{18}) in test-2.

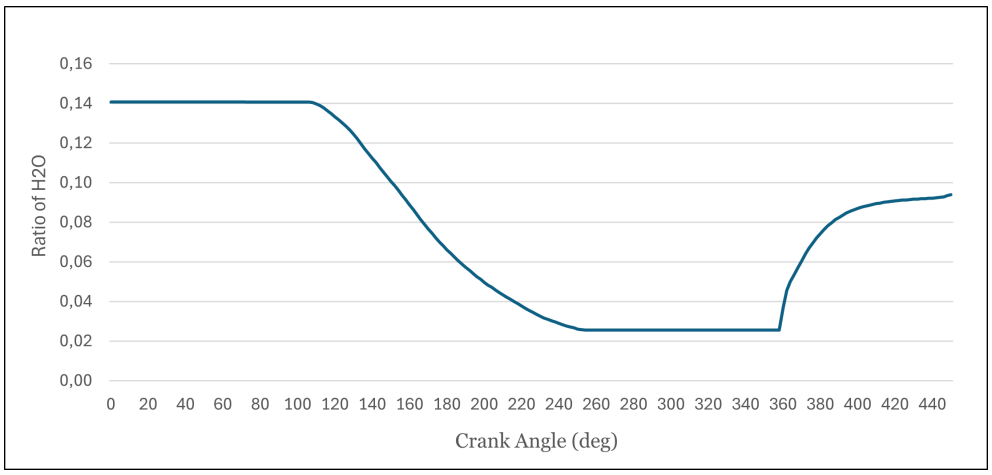

Figure C.13: In cylinder ratio of water vapor (H_2O) in test-2.

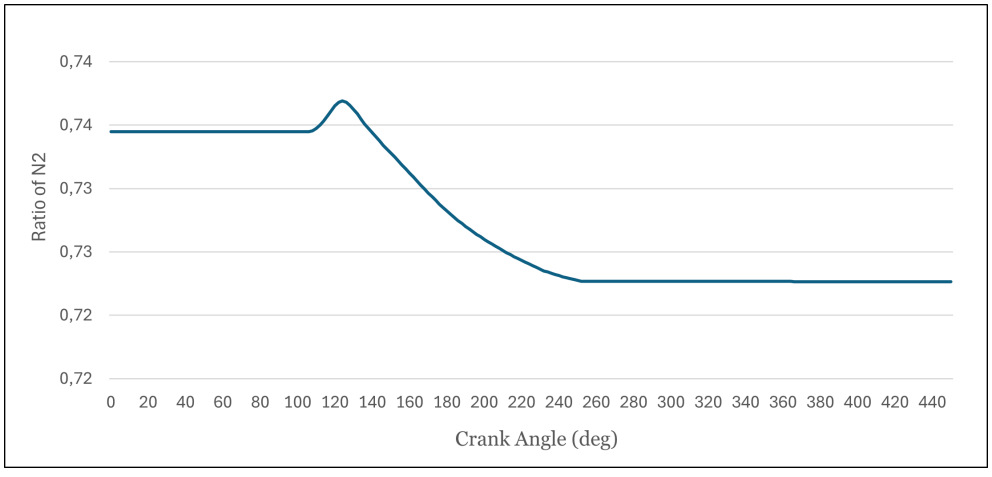

Figure C.14: In cylinder ratio of nitrogen (N_2) in test-2.

C.4 Test-3

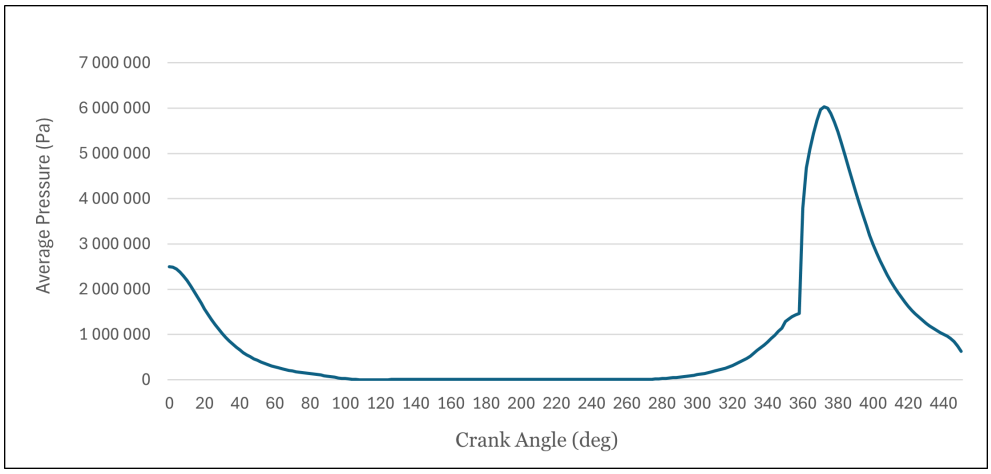

Figure C.15: In cylinder pressure in test-3.

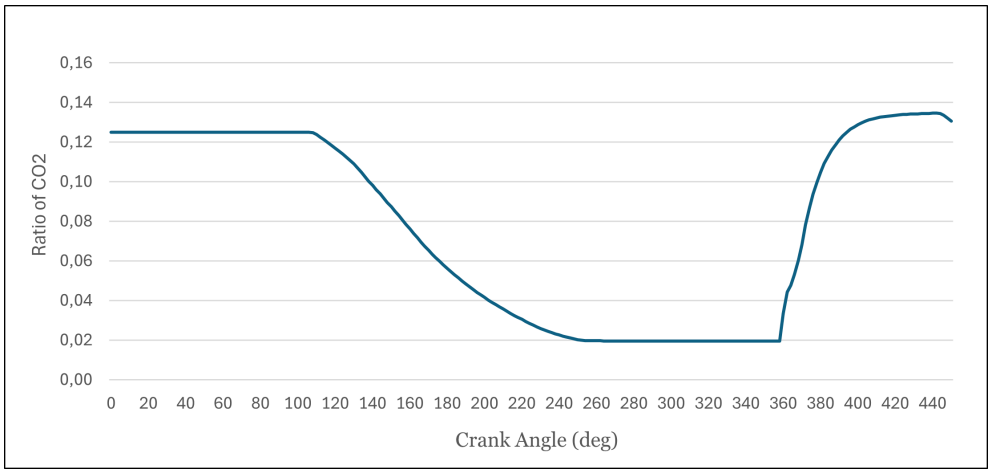

Figure C.16: In cylinder ratio of Carbon dioxide (CO_2) in test-3.

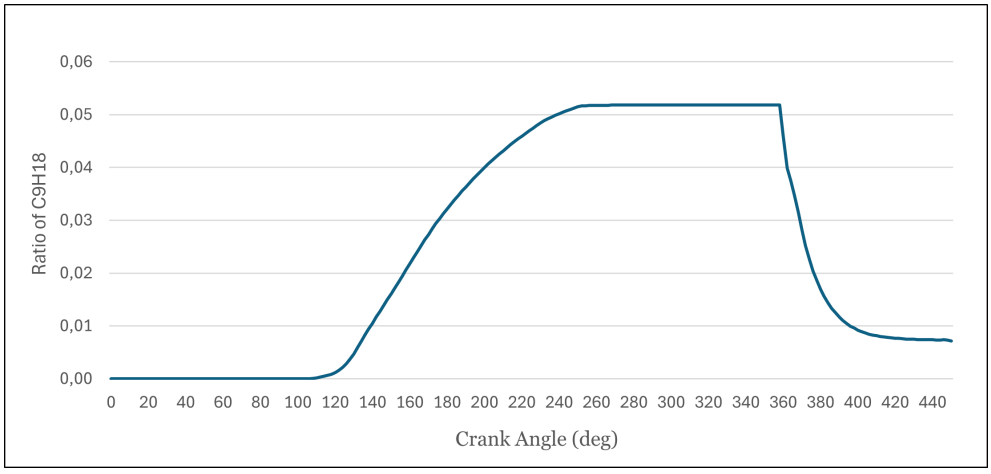

Figure C.17: In cylinder ratio of octane (C_8H_{18}) in test-3.

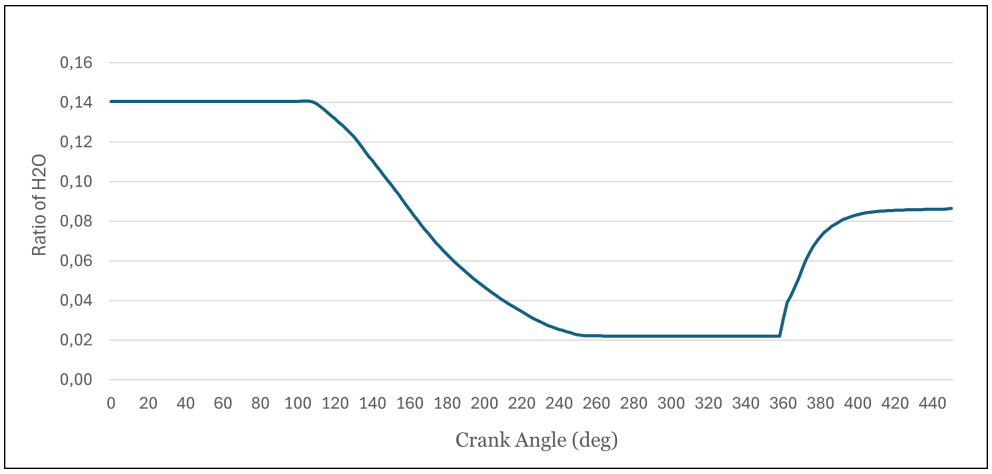

Figure C.18: In cylinder ratio of water vapor (H_2O) in test-3.

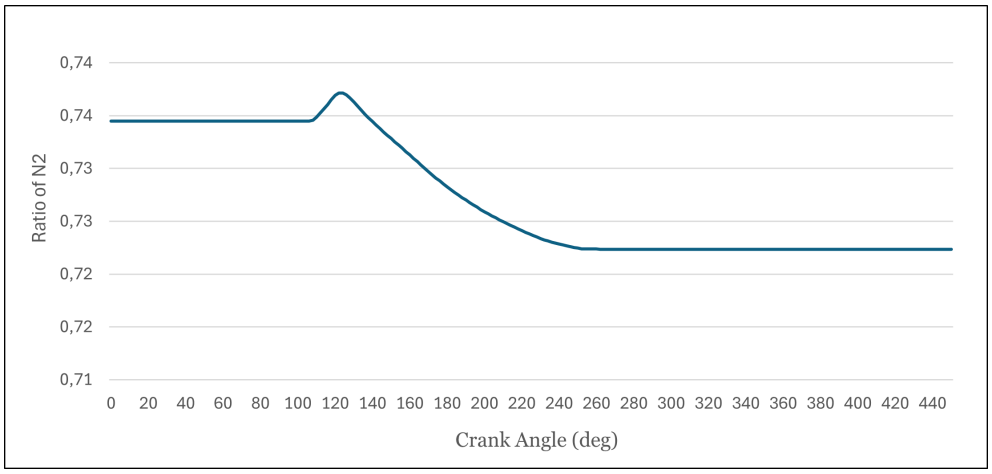

Figure C.19: In cylinder ratio of nitrogen (N_2) in test-3.

C.5 Test-4

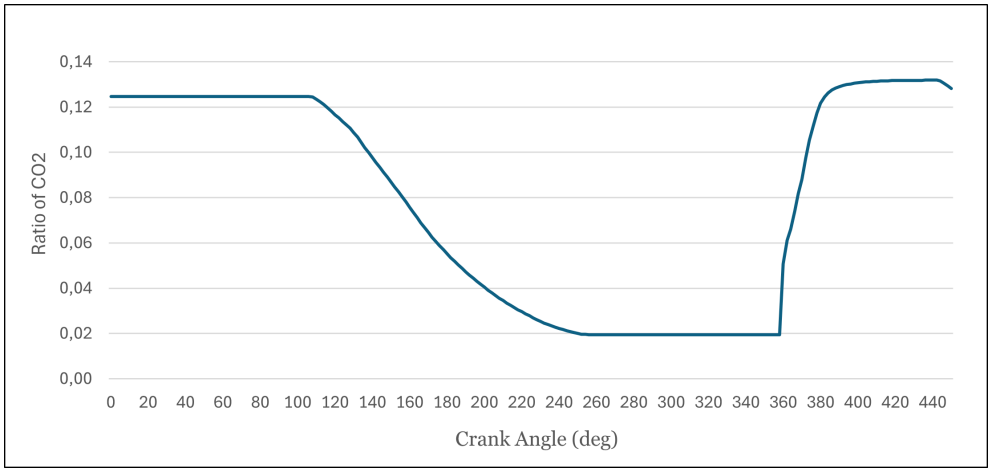

Figure C.20: In cylinder ratio of Carbon dioxide (CO_2) in test-4.

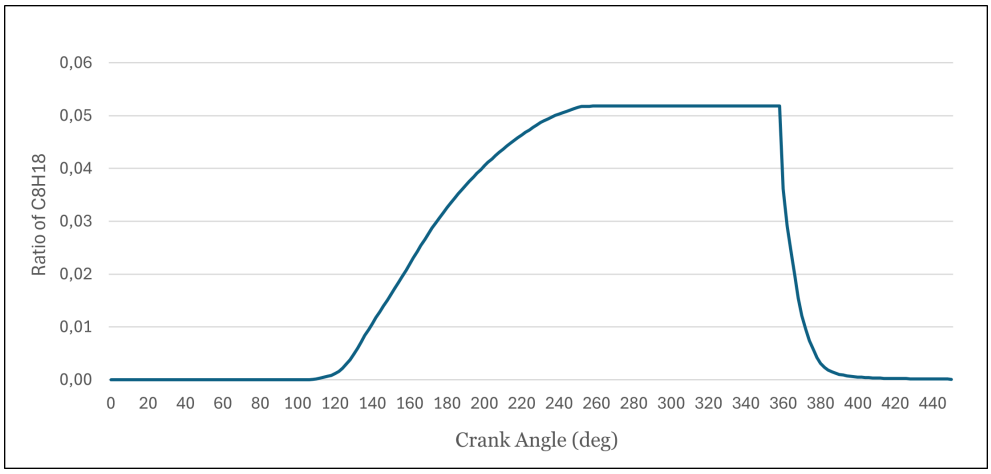

Figure C.21: In cylinder ratio of octane (C_8H_{18}) in test-4.

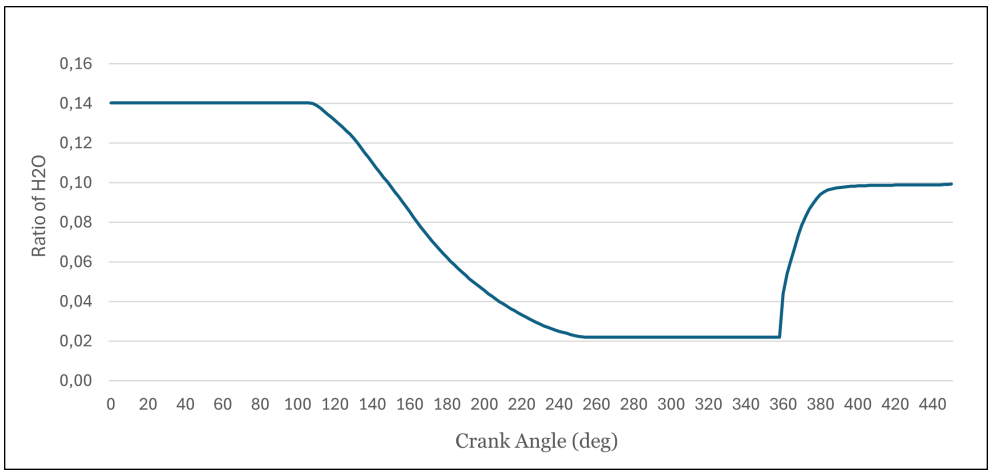

Figure C.22: In cylinder ratio of water vapor (H_2O) in test-4.

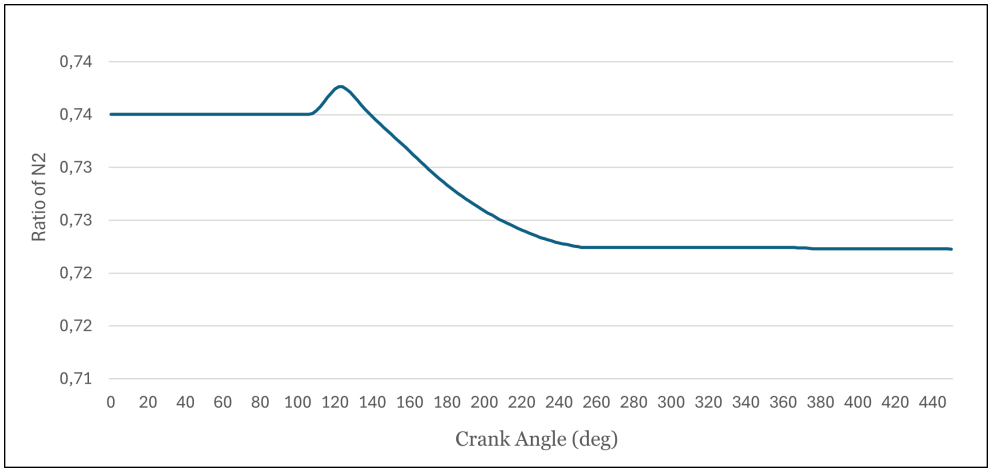

Figure C.23: In cylinder ratio of nitrogen (N_2) in test-4.

C.6 Test-5

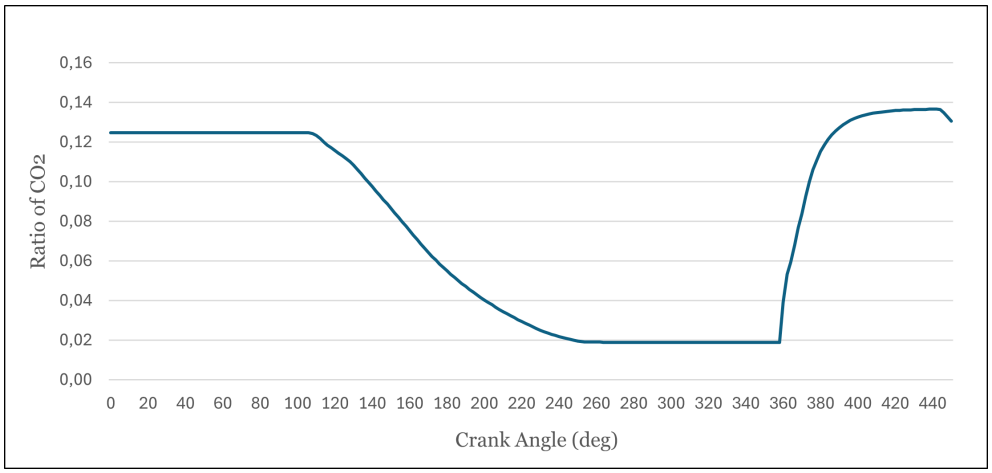

Figure C.24: In cylinder ratio of Carbon dioxide (CO_2) in test-5.

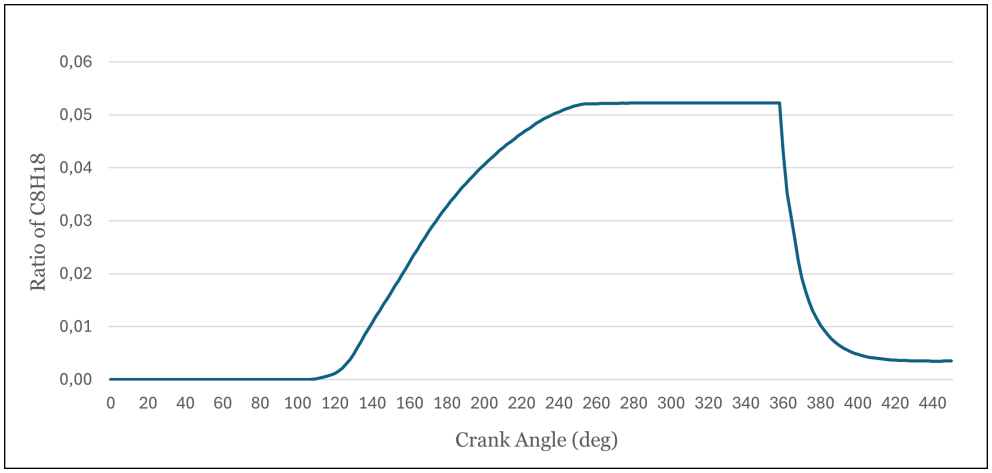

Figure C.25: In cylinder ratio of octane (C_8H_{18}) in test-5.

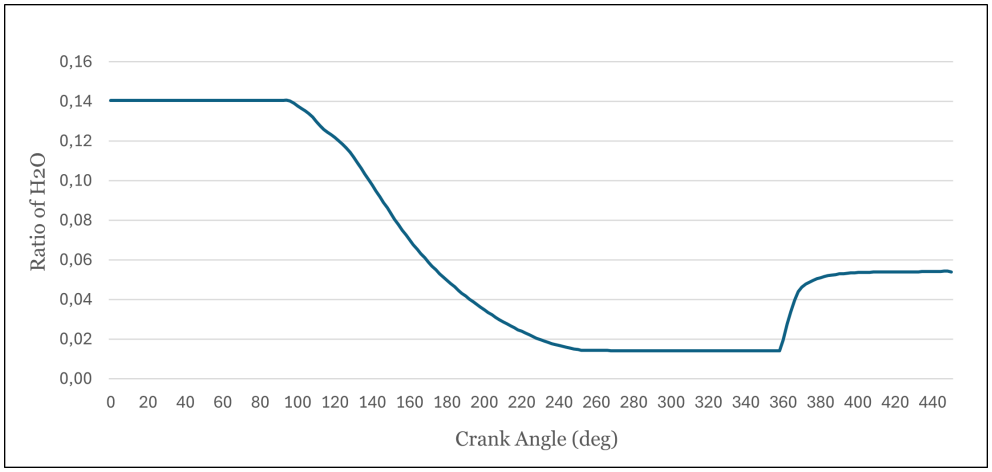

Figure C.26: In cylinder ratio of water vapor (H_2O) in test-5.

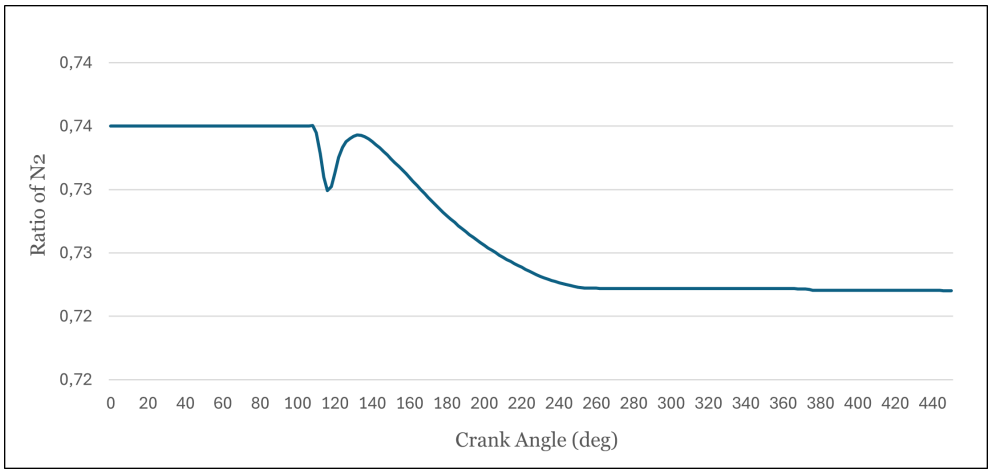

Figure C.27: In cylinder ratio of nitrogen (N_2) in test-5.